Title

A molecular interactome of the glioblastoma perivascular niche reveals integrin binding sialoprotein as a mediator of tumor cell migration

Journal

Cell Reports, 41(3)

ISSN

2639-1856

Authors

Ghochani, Yasmin
Muthukrishnan, Sree Deepthi
Sohrabi, Alireza
et al.

Publication Date

2022-10-01

DOI

10.1016/j.celrep.2022.111511

Peer reviewed

HHS Public Access

Author manuscript

Cell Rep. Author manuscript; available in PMC 2022 November 08.

Published in final edited form as:

Cell Rep. 2022 October 18; 41(3): 111511. doi:10.1016/j.celrep.2022.111511.

A molecular interactome of the glioblastoma perivascular niche reveals integrin binding sialoprotein as a mediator of tumor cell migration

Yasmin Ghochani[1,3,12], **Sree Deepthi Muthukrishnan**[1,12], **Alireza Sohrabi**[2], **Riki Kawaguchi**[1,3], **Michael C. Condro**[1], **Soniya Bastola**[1,2], **Fuying Gao**[1,3], **Yue Qin**[1,3], **Jack Mottahedeh**[1], **M. Luisa Iruela-Arispe**[4], **Nagesh Rao**[5], **Dan R. Laks**[1,6], **Linda M. Liau**[7], **Gary W. Mathern**[1,7], **Steven A. Goldman**[8], **S. Thomas Carmichael**[3], **Ichiro Nakano**[9], **Giovanni Coppola**[1], **Stephanie K. Seidlits**[2,11,*], **Harley I. Kornblum**[1,10,12,13,*]

[1]Department of Psychiatry and the Semel Institute for Neuroscience and Behavior, David Geffen School of Medicine at UCLA, 635 Charles E. Young Drive South, Los Angeles, CA 90095, USA

[2]Department of Bioengineering, UCLA, 410 Westwood Plaza, Los Angeles, CA 90095, USA

[3]Department of Neurology, David Geffen School of Medicine at UCLA, 635 Charles E. Young Drive South, Los Angeles, CA 90095, USA

[4]Department of Cell and Developmental Biology, Northwestern University, 303 E. Superior St. SQBRC 8-300, Chicago, IL 60611, USA

[5]Department of Pathology and Laboratory Medicine, David Geffen School of Medicine at UCLA, 635 Charles E. Young Drive South, Los Angeles, CA 90095, USA

[6]Voyager Therapeutics, 64 Sidney St., Cambridge, MA 02139, USA

[7]Department of Neurosurgery, David Geffen School of Medicine at UCLA, 635 Charles E. Young Drive South, Los Angeles, CA 90095, USA

*Correspondence: seidlits@utexas.edu (S.K.S.), hkornblum@mednet.ucla.edu (H.I.K.).

AUTHOR CONTRIBUTIONS

Y.G., S.D.M., A.S., M.C.C., and S.B. performed the experiments and collected and analyzed the data. N.R. performed the cytogenetic experiments. J.M. and D.R.L. contributed to methods and reagents and analyzed the data. L.M.L. and G.W.M. provided clinical samples. F.G., Y.Q., and R.K. performed the bioinformatics analysis. M.L.I.-A., I.N., G.C., S.A.G., S.T.C., S.K.S., and H.I.K. conceptualized and supervised the study. Y.G., S.D.M., A.S., and H.I.K. wrote, edited, and revised the manuscript.

DECLARATION OF INTERESTS

S.T.C. is member of the Scientific Advisory Board of Athersys, Fibrobiologics, and San Bio. His laboratory received research support from BrainQ and Universal Cells. S.A.G. is a part-time employee, officer, and stock-holder of Sana Biotechnology, a cell therapy company, and his lab receives sponsored research support from Sana. He is also a co-founder and advisor to CNS2, another cell therapy company from which his lab receives support and in which he holds equity. None of the work described in this paper overlaps with their work with these companies.

SUPPLEMENTAL INFORMATION

Supplemental information can be found online at https://doi.org/10.1016/j.celrep.2022.111511.

INCLUSION AND DIVERSITY

One or more of the authors of this paper self-identifies as an underrepresented ethnic minority in their field of research or within their geographical location. One or more of the authors of this paper self-identifies as a gender minority in their field of research.

[8]Center for Translational Neuromedicine, University of Rochester Medical Center and University of Copenhagen Faculty of Medical Sciences, 601 Elmwood Ave, Box 645, Rochester, NY 14642, USA

[9]Research and Development Center for Precision Medicine, Tsukuba University, Tsukuba, Japan

[10]Departments of Pediatrics and Pharmacology, David Geffen School of Medicine at UCLA, 635 Charles E. Young Drive South, Los Angeles, CA 90095, USA

[11]Present address: The University of Texas at Austin, Department of Cellular and Biomolecular Engineering, Austin, TX 78712, USA

[12]These authors contributed equally

[13]Lead contact

SUMMARY

Glioblastoma (GBM) is characterized by extensive microvascular hyperproliferation. In addition to supplying blood to the tumor, GBM vessels also provide trophic support to glioma cells and serve as conduits for migration into the surrounding brain, promoting recurrence. Here, we enrich CD31-expressing glioma vascular cells (GVCs) and A2B5-expressing glioma tumor cells (GTCs) from primary GBM and use RNA sequencing to create a comprehensive molecular interaction map of the secreted and extracellular factors elaborated by GVCs that can interact with receptors and membrane molecules on GTCs. To validate our findings, we utilize functional assays, including a hydrogel-based migration assay and *in vivo* mouse models to demonstrate that one identified factor, the little-studied integrin binding sialoprotein (IBSP), enhances tumor growth and promotes the migration of GTCs along the vasculature. This perivascular niche interactome will serve as a resource to the research community in defining the potential functions of the GBM vasculature.

In brief

Ghochani et al., report the identification of a molecular interactome of vascular-derived angiocrines and their putative interacting partners on tumor cells in glioblastoma and identify an important role for vascular-enriched integrin binding sialoprotein (IBSP) in mediating tumor cell migration, proliferation, and mesenchymal transition.

Graphical Abstract

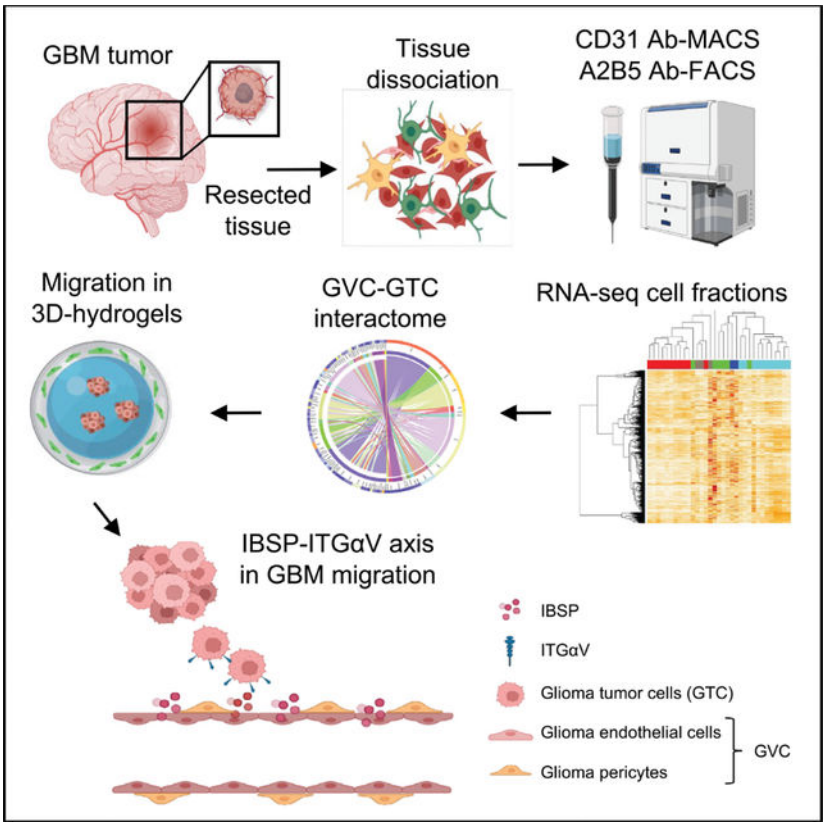

INTRODUCTION

Glioblastoma (GBM) is the most common primary and lethal primary brain tumor, inevitably recurring following the standard therapies of surgery, radiation, and chemotherapy with temozolomide (Stupp et al., 2015). One of the primary hallmarks of GBM is extensive microvascular proliferation, characterized by heterogeneous, dysfunctional vessels with variable diameter and permeability (Brat and Van Meir, 2001; Das and Marsden, 2013).

The GBM vasculature largely consists of endothelial cells, pericytes, and perivascular immune cells and plays a critical role in the maintenance of blood flow to the tumor cells (Charles and Holland, 2010). There is increasing evidence that vasculature can play other important roles in GBM. For example, vascular cells are known to provide a means by which GBM cells migrate out of the tumor, which then serve as the seeds of recurrence following therapy (Farin et al., 2006; Griveau et al., 2018). In experimental models, vascular cells have been demonstrated to provide trophic support to tumor cells, outside of their role in supplying blood, including allowing them to survive therapeutic insults, such as radiation (Garcia-Barros et al., 2003; Calabrese et al., 2007; Charles et al., 2010; Yan et al., 2014; Brooks and Parrinello, 2017).

While a great deal is known about how GBM cells induce the ingrowth and elaboration of the GBM vasculature, few studies have highlighted the factors that the vasculature produces that may act on the tumor cells, and how tumor cells may respond to these factors (Bao et

al., 2006; Brat and Van Meir, 2001; Gilbertson and Rich, 2007). To investigate the potential tumor-promoting roles of the microvasculature, early studies have tried to identify a core set of dysregulated genes associated with aberrant GBM vessels compared with normal brain vessels (Charalambous et al., 2005, 2007; Pen et al., 2007; Dieterich et al., 2012). Although these studies provided a great deal of information, due to technical limitations they did not yield a comprehensive map of the factors elaborated by GBM vasculature.

In this study, we have overcome some of these technical limitations by performing RNA sequencing of highly enriched vascular and tumor cells from primary GBM tumors. We have created an extensive map of interactions among potentially secreted and extracellular factors elaborated by the GBM vascular cells (GVCs) and receptors and other membrane-bound molecules on GBM tumor cells (GTCs), which represents a key resource for the research community. To validate our findings, we demonstrate that one of our identified factors, the little-studied IBSP, provides trophic support and promotes the migration of GTCs along the vasculature.

RESULTS

Transcriptomic profiling of cells expressing CD31 or A2B5 from non-transformed cortices and primary GBM uncovers tumor-specific dysregulated genes

To delineate the molecular interactions between the perivascular niche (PVN) and tumor cells, we developed a strategy involving the sequential enrichment of CD31+ (PECAM1) vascular cells (GVCs) and A2B5+ tumor cells (GTCs) from non-transformed brain cortical samples (n = 5) and GBM samples (n = 11). Of the 11 GBM samples, we collected RNA from unsorted tumor (GBM), GVCs and GTCs from 5 samples, and only unsorted tumor and GVC fraction from two samples for RNA sequencing. Four samples were excluded from the analysis as they were not primary GBM samples or had poor quality. Information on TCGA molecular classification and sample characteristics are described in the STAR methods. We selected cell-type-specific markers based on three criteria: (1) virtually all endothelial cells are CD31+ and tumor-initiating cells are contained within the A2B5+ fraction (Auvergne et al., 2013; Tchoghandjian et al., 2010), (2) cell surface markers can be used to isolate and enrich for cell types by MACS and FACS sorting, and (3) they can be used to enrich for their non-neoplastic counterparts: normal brain glial progenitor cells (BGPCs) and normal brain vascular cells (BVCs) allowing for direct comparisons (Figure 1A).

To validate that the A2B5+ fraction is enriched for tumor-initiating cells, we first performed cytogenetic analysis using dual color fluorescence *in situ* hybridization of the unsorted GBM and GTC fractions from the same tumor. A2B5+ cells harbored the major chromosomal alterations of the parent tumor and showed enrichment of EGFR transcript in tumors with EGFR amplification (Figures S1A and S1B). Differential gene expression analysis (DEA) and hierarchical clustering of each sample versus combined expression of non-neoplastic gray and white matter revealed similarity in expression profiles within each cellular fraction, while distinguishing each individual fraction (Figure 1B). Specifically, examination of differential gene expression of the GTCs versus BGPCs identified 1,471 transcripts that were significantly enriched and 1,092 that were significantly depleted in GTCs (Table S1A).

We utilized Ingenuity Pathway Analysis (IPA) to identify significantly enriched diseases or functions associated with the differentially expressed genes in GTC versus BGPC fractions. Significant upregulation of tumor pathways promoting proliferation, survival, CNS neoplasia and gliomagenesis, and downregulation of normal brain functions such as learning and cognition supported the neoplastic nature of the isolated GTCs, and the inclusion of the tumor propagating cells within the A2B5+ fraction (Figure S1C; Table S1B). We further evaluated the expression of known astroglial- and oligodendroglialprogenitor (OPC) markers, neural stem/progenitor cell markers, and cancer stem-like cell markers in the sorted and unsorted fractions using direct expression intensity analyses (FPKM values) and differential expression (Figure S1D). GTCs were enriched for the OPC markers OLIG2, CSPG4, SOX10, and NKX2–2 compared with the unsorted parent GBM tumors and, as expected, these markers were also enriched in BGPCs (Figure 1C). GTCs also exhibited significant upregulation of STAT3 and GFAP, astrocyte-enriched genes, and progenitor cell markers KLF4 and MSI1 compared with unsorted GBM. BGPCs, however, did not significantly express STAT3, GFAP, or MSI1 markers compared with GBM samples or their A2B5+ fractions. Finally, both the parent GBM and their GTC fractions had significantly elevated expression of the neural progenitor marker NES, and cancer stem cell regulator MYC compared with the BGPCs, consistent with the hypothesis that the A2B5+ GTCs contain the tumor stem/progenitor-like character. Taken together, these findings strongly support the notion that the A2B5+ fraction is highly enriched for tumor cells with stem-like properties.

Molecular characterization and identification of GVC-specific factors

To validate the identity of CD31-enriched GVC fraction, we examined endothelial and pericyte markers, both of which were significantly upregulated in GVC fraction versus the parent tumors (Figure 1D). As expected, GVCs showed significant downregulation of the astrocyte, oligodendrocyte, and neuronal markers GFAP, OLIG2, and RBFOX3 (NeuN), respectively. The presence of pericyte-like markers within this fraction could indicate that pericytes remained tightly bound to endothelial cells during the enrichment process or that some genes generally associated with pericytes are expressed by CD31+ GVCs.

Differential analysis identified 445 genes enriched in GVCs compared with BVCs ($p < 0.005$) and captured known regulators of the GBM-perivascular interaction such as ANGPT2 (Scholz et al., 2016; Stratmann et al., 1998), VEGF-A induced endothelial genes ESM1, NOX4, PXDN (Dieterich et al., 2012), and TGFβR1 (Krishnan et al., 2015) (Figure 2A; Table S2A). In addition, examination of the significantly activated upstream regulators of GVCs revealed known vascular regulators in GBM, such as TGF-β, VEGF, HIF1α, NOS2, various RTKs, SPP1 and endothelin-1 ($p = 0.01$) (Dieterich et al., 2012; Jeon et al., 2014; Musumeci et al., 2015), and IL1A/B (IL1A, $p = 1.6 \times 10^{-5}$; IL1B, $p = 7.8 \times 10^{-7}$) (Figure 2A; Table S2B). We also further validated the expression of the top 10 differentially expressed GVC factors in publicly available single-cell RNA sequencing dataset of CD31+ tumor endothelial cells enriched from core and edge tissue of primary GBM samples (Figure S2A) (Xie et al., 2021). We found that several GVC-enriched genes were expressed in EC clusters from both core and edge of the tumors, with IBSP showing greatest enrichment in an edge-derived EC cluster (Figure S2B). IPA analysis of GVC

versus BVC transcriptomes revealed significant enrichment of GO terms related to glioma invasiveness and proliferation, and negative association with tumor necrosis and cell death (Figure 2B; Tables S2B and S2C). Thus, our unbiased transcriptomic analysis of the freshly isolated GVC provides the opportunity for investigation of multiple dysregulated genes and pathways within the GBM PVN.

GTC-GVC molecular interactome reaffirms a prominent role for PVN regulation of GBM migration

Because of the high degree of enrichment of GO terms associated with invasiveness and migration, we sought to determine whether GVC-secreted factors could directly influence invasive capacity of GBM cells. We used a previously validated hyaluronic acid (HA)-based hydrogel system that supports the 3D culture of gliomaspheres to assess various parameters, such as proliferation, apoptosis, viability, and treatment resistance (Xiao et al., 2018a, 2018b, 2020). To assess the migration of gliomasphere cells in the presence of vascular cells, we separately encapsulated GBM gliomaspheres and short-term primary cultures of GVCs or BVCs, placing them in close proximity to each other (Figure 2C). We first validated the vascular characteristics of cultured GVCs by CD31 immunostaining at different passages, and using a DiI-Ac-LDL uptake assay (Figure S2C). RNA sequencing of GVC culture showed expression of known endothelial markers such as PECAM1, VE-CADHERIN (CDH5), KDR, VWF (FPKM values in Figure S2D). GVCs expressed some markers of pericyte lineage, such as PDGFRB, CSPG4, ACTA2, MCAM, and CD248, but did not express immune cell markers, including CD45 (PTPRC), CD14, and ITGAM, indicating that cultured GVCs could be of a mixed endothelial/pericyte identity (Figure S2D). Gliomaspheres cultured alone or in presence of BVCs (human brain vascular endothelial cells) demonstrated different migration potential (measured as the distance of cell movement away from the sphere edge), with no migration (0 ± 0 μm) or minimal migration (39.9 ± 21.8 mm) ($p < 0.0001$), respectively. Shape factor analysis (where 1 indicates no migratory potential and 0 indicates high migratory potential) revealed non-migratory (0.9 ± 0.02) or mildly migratory (0.5 ± 0.1) ($p < 0.0001$) in the presence of BVCs (Figures 2D and 2E). However, gliomaspheres co-encapsulated with GVCs showed significantly increased migration distance of 116.2 ± 30.4 μm ($p < 0.0001$) and aggressive migratory potential with shape factor average of 0.09 ± 0.04 ($p < 0.0001$) (Figures 2D and 2E). These findings indicate that factors elaborated by GVCs promote GBM migration.

Given that our functional 3D *in vitro* assays demonstrated increased GBM migratory potential in the presence of GVCs, and our transcriptomic analysis showed enrichment of promigration/invasion-related pathways, we sought to identify specific angiocrines elaborated by GBM vasculature that can influence tumor cell biology. A putative GTC-GVC molecular interactome was developed by generating unique transcriptional profiles to identify specific cues in GVCs that can mediate the pro-migratory effect on GTCs. We began our analysis by scrutinizing the 113 GVC extracellular factors and the 331 GTC plasma membrane (PM) proteins, exclusively, which were differentially regulated as compared with BVCs and BGPCs. Differential expression of angiocrines in GVCs versus BVCs are shown in Table S3A, and differential expression of GTCs versus BGPCs PM proteins are shown in Table S3B. Utilizing a combination of manual and IPA software

curation focused on previously reported direct and indirect protein-protein interactions, we identified 24 interacting groups encompassing hormones, extracellular matrix components, such as laminins, collagens, and matrix metalloproteinases, and members of the small integrin-binding ligand N-linked glycoprotein (SIBLING) family of proteins (Figure 3A). In the case of the SIBLING proteins, the interaction partners are mostly those previously reported for the osteopontin (OPN)-encoding gene, SPP1 (Lamour et al., 2015). However, due to conservation of various functional motifs, such as post-translational modification motifs, acidic amino acids, and the RGD (Arg-Gly-Asp) motif, as well as the much more prominent and significant upregulation of another member of this family, IBSP compared with SPP1, we extended the interaction unit to include all upregulated members of the SIBLING family (Bellahcène et al., 2008). As expected, IPA of the diseases and functions associated with the genes within this interactome revealed cellular movement and migration as the most significantly upregulated, followed by angiogenesis, and cellular proliferation (Figure 3B).

The interactome described above assumed that both the extracellular factors/ligands and the PM proteins/receptors must be dysregulated for their interaction to be of consequence in promoting tumor migration. To obtain a more comprehensive view of all the GVC angiocrines and their putative interaction with all the GTC membrane proteins, we utilized FPKM expression intensity values and considered those with FPKM > 1 for at least 1/3 of the samples to account for the heterogeneity that exists among GBM. We identified 552 GVC extracellular factors and 1,254 GTC PM genes. GVC extracellular factors FPKM (1), GTC PM proteins FPKM (2), and our comprehensive PVN interactome by FPKM expression units (3) are shown in Table S4, where FPKM > 4 are highlighted in red (collagen and complement factor interactions are not shown). We eliminated factors that were expressed by both GVCs and GTCs with an FPKM difference of <4, thus narrowing the interactome to putative GTC dependence on GVCs, and not GTC autocrine signaling. We identified 135 angiocrines that had at least one, but often multiple, putative GTC-interacting partners. Grouped into different functional categories, the circos plots demonstrate the angiocrines on the right hemi-circle and their color-coded GTC interacting partners on the left for easy identification of GTC-GVC tumor-angiocrine interactions, with the outer circles demonstrating expression levels of various factors (Figure S3A). A representative plot depicting the ECM components, SIBLINGS, transporters, and membrane components is shown in Figure 3C. IPA annotation of functions associated with this comprehensive interactome (Figure 3D; Table S4) confirmed that the most significantly enriched GO_Term is cellular migration and movement, again indicating that promotion of tumor invasion is a likely function of the interacting proteins. Furthermore, there was a modest enrichment of terms associated with tumor proliferation, suggesting a potential role for the angiocrines in mediating this process. Within this comprehensive interactome, we found many previously reported PVN angiocrine-receptor interactions validating our experimental approach (Figure S3B). In addition, we identified multiple putative interactions, such as inhibins of the TGF-β superfamily, ECM small leucine-rich proteoglycan family of proteins, such as lumican, biglycan, and nidogen, basement membrane components, along with their putative binding partners, demonstrating the complexity of the signaling emanating from the PVN.

IBSP regulates tumor cell migration and proliferation and induces a mesenchymal signature

Since tumor invasion and migration-related signaling was highly enriched within the PVN interactome, we tested a subset of candidate angiocrines that were upregulated in GVCs compared with BVCs: DMP1, ESM1, MMP8, MMP12, lumican, inhibinB-A, WNT5A, and IBSP in promoting migration of GTCs using the 3D HA-hydrogel system. Since the GBM microenvironment is rich in RGD-containing factors, which are necessary for migration, and that GTCs express high levels of integrin receptors, we used an RGD peptide-conjugated HA culture scaffold as our positive control, and all factors were studied on the background of RGD-conjugated hydrogels, using a cysteine-only hydrogel with no integrin-binding sites as a negative control (Figure 3E). Of the angiocrines assessed, IBSP (integrin binding sialoprotein, BSPII) peptide showed the most significant effect on migration above the baseline distance promoted by the RGD control (Figures 3E, 3F, S3C, and S3D).

Within the PVN interactome, multiple SIBLING family members were highly upregulated in GVCs compared with BVCs. However, IBSP was the most upregulated member of this family (logFC of 13, $p = 0.0001$) and almost exclusively expressed by GVCs (FPKM = 50.1 versus GTC FPKM = 2.4) (Figures S4A–S4C). Analysis of TCGA samples showed that IBSP mRNA was highly enriched in the tumor compared with non-tumor samples, and more significantly upregulated in IDH-wild-type (WT) tumors relative to IDH-mutant tumors (Figure 4A). IBSP expression was also highly enriched in the microvascular-enriched region compared with the cellular and infiltrating tumor in the samples assessed from the IVY_GAP database (Figure 4B). Immunohistochemistry of two primary GBM tissues validated the vascular expression of IBSP protein (Figures 4C and S4D). Vascular expression of the IBSP transcript was also confirmed by fluorescent *in situ* hybridization (RNAscope) with some apparent co-expression in PECAM-1 mRNA-expressing endothelial cells and PDGFRβ mRNA-expressing presumptive pericytes (Figure 4D).

To determine whether IBSP expression was associated with patient outcome, we utilized Gliovis (Bowman et al., 2017) to assess GBM patient survival correlation with IBSP expression within different tumor subtypes. Although IBSP mRNA was expressed highly in all molecular subtypes, we found that elevated IBSP correlated with diminished survival only in the proneural subtype of IDH-WT tumors ($p = 0.0003$) (Figures 4E and S4E). Because of the enrichment of terms associated with proliferation of tumor cells, we added IBSP to gliomasphere cultures from all three subtypes, and found elevated cell numbers only in the gliomaspheres that had previously been characterized as proneural (Figure 4F), accompanied by an increase in BrdU incorporation (Figure 4F, inset). These findings indicate that IBSP could play an important role in regulating proliferation of proneural IDH-WT GBM.

To determine the molecular basis of IBSP-induced effects, we treated two proneural GBM cultures (HK157 and HK217) with IBSP and profiled gene expression by microarray. DEA revealed upregulation of genes associated with mesenchymal phenotype, such as CD44 ($p < 2.26 \times 10^{-9}$) and MMP1 ($p < 3.03 \times 10^{-11}$) in IBSP-treated tumors, indicating a shift toward mesenchymal gene signature (Figure S5A). The complete IBSP versus CTRL DEA (FDR < 0.001 (A)), significantly enriched canonical pathways ($p < 0.05$ (B)), upstream

regulators ($p < 0.05$ (C)), and diseases and functions associated with DEA ($p < 1.5 \times 10^{-6}$ (D)) can be found in Table S5. Canonical pathway analysis revealed a significant enrichment of FAK and integrin signaling, known regulators of glioma invasiveness. In addition, there was also significant enrichment of paxillin, IGF-1, and ephrin receptor signaling, which could potentially play a role in PVN-induced acquisition of a more aggressive and invasive phenotype by GBM cells (Figure 5A). Furthermore, IPA upstream regulator analysis predicted that NF-κB, STAT3, and HIF1α were significantly activated (Figure 5B). Based on these results, we reasoned that IBSP may induce a mesenchymal shift in tumor cells resulting in the observed migratory phenotype described above. To further test this, we classified the CTRL and IBSP-treated cells according to TCGA classification of gliomaspheres (Laks et al., 2016) (Figure 5C). As expected, when we performed PCA of genes used to categorize samples of the tumors in the TCGA database (2008) (Verhaak et al., 2010), these samples separated according to subclass (classical, proneural, mesenchymal). We then superimposed the gene expression signatures of our control and treated gliomasphere samples. This superimposition clearly demonstrated the movement of the samples from a more proneural state toward a more mesenchymal signature upon IBSP treatment, particularly when comparing each CTRL with its paired IBSP sample. Although the HK157 GBM line exhibited a more robust phenotype, HK217 also displayed a similar expression profile upon IBSP treatment as its DEA (FDR < 0.05) significantly overlapped with the HK157 DEA (p value of overlap = 1.3×10^{-243}).

To assess the behavior of IBSP-treated cells in the *in vivo* microenvironment, we pretreated two gliomasphere lines known to exhibit robust tumor formation following transplantation, 1005 and 1051, for 3 days with IBSP and examined the tumors in mouse brain xenografts (Figure 5D). As demonstrated by staining for human cells 4 weeks following implantation, IBSP-treated samples produced overtly larger and more invasive tumors (Figure 5E), an impression substantiated by quantitative analysis of tumor area (Figure 5F). Furthermore, to assess whether IBSP potentially induced a mesenchymal shift in the tumors, we immunostained for the known mesenchymal markers vimentin, CD44, and YKL40 (CHI3L1), and the proneural marker Olig2. Both the IBSP-treated tumors had significantly increased expression of the mesenchymal markers and decreased expression of Olig2 (Figures 5G–5I, S5B, and S5C). Our functional data thus far indicate that IBSP promotes GTC migration, proliferation of a subset of proneural GBM lines, and a mesenchymal shift in gene expression.

ITG0αV mediates the pro-migratory and pro-proliferative effects of IBSP

Since IBSP is a known integrin-binding protein, we next sought to determine which integrins might be important for its function. From the comprehensive interactome, we identified a number of expressed integrins (Figure 6A), some of which were previously shown to interact with the SIBLING ligands. For example, ITGαVβ3 and ITGαVβ5 interact with IBSP to promote breast cancer proliferation and invasion, respectively (Sung et al., 1998). To determine whether the expressed integrins were relevant for IBSP function, we performed high-throughput shRNA screening based on migration capacity in hydrogels in the presence of IBSP (Figure 6B). Infection with at least one of the clones for ITGαV, ITGβ3, ITGα6, ITGα7, ITGβ8, and ITGα1 resulted in significantly reduced GTC

dispersion in hydrogel ($3 \leq N \leq 8$) (Figure 6B). However, of all the integrins, ITGβ8 and ITGαV showed the highest expression in GTCs (Figure 6A). IBSP is known to promote tumor invasion through its interactions with the ITGαV receptor in other cancers (Karadag et al., 2004; Sung et al., 1998). We therefore selected this subunit as the leading α-integrin candidate. Fluorescent *in situ* hybridization of patient tumor tissue revealed that ITGαV is expressed by tumor cells, including those adjacent to IBSP-expressing vasculature (Figure S6A). Next, we assessed its role in mediating the effects of IBSP on migration of three different primary gliomasphere lines representing proneural (HK217 and HK301) and mesenchymal (HK280) expression groups using a specific ITGαV-blocking antibody. As expected, IBSP induced migration in all three gliomasphere lines tested (Figure 6C), an effect completely abolished by concomitant treatment with the ITGαV blocking antibody (Figures 6D and S6B). To validate the specificity of this effect, we knocked down ITGαV expression in tumor cells with two separate shRNAs. Validation of knockdown efficiency of both shRNAs by qRT-PCR and immunoblotting is shown in Figure S6C, with shITGαV_150 showing the greatest reduction in both RNA and protein. We found that ITGαV knockdown with both constructs reversed the pro-migratory effects of IBSP. However, it is important to note that shITGαV_150 alone abrogated the pro-migratory effect induced by RGD, indicating that ITGαV may be required for all RGD-induced migration (Figures 6E, 6F, and S6D). We also assessed whether ITGαV mediates the pro-proliferative effects and promotes mesenchymal signature induced by IBSP. ITGαV knockdown (shRNA_150) cells diminished the proliferative effect of IBSP in two proneural GBM lines (HK408 and HK217) tested (Figures S6E and S6F). qRT-PCR analysis of proneural (OLIG2 and SOX2) and mesenchymal markers (CD44 and VIM) in ITGαV knockdown cells showed reduced expression of mesenchymal markers in response to IBSP relative to control cells (Figure S6G). These results indicate that ITGαV acts as the predominant α-integrin receptor for IBSP in GBM tumors.

Endogenous IBSP regulates tumor growth and migration

Our functional studies indicate that exogenously added IBSP influences GBM proliferation and migration. To examine the effects of endogenous, vascular-derived IBSP, we first utilized our hydrogel co-culture system. A shRNA-mediated knockdown of IBSP was performed using three different validated constructs in cultured GVCs (Figures S7A–S7C). Knockdown of IBSP in GVCs resulted in dramatically diminished migration of the co-cultured GTCs compared with cells infected with control viruses or positive control cells (Figures 7A, 7B, and S7D). Neither the soluble form of IBSP nor IBSP knockdown had any significant effect on GVC proliferation (Figure S7E), thus eliminating the likelihood that IBSP altered GVC numbers which might have contributed to an increase in other migration-promoting factors in the co-culture system.

Next, we sought to determine whether endogenous IBSP plays a role in promoting tumor growth and migration *in vivo*. We utilized a murine glioma cell line harboring activated NRAS-G12V, and TP53 and ATRX inactivating mutations (Nunez et al., 2019) that expressed GFP-firefly luciferase, which we transplanted into *Ibsp* WT and KO mice (Malaval et al., 2008). Quantitation of tumor growth by bioluminescence imaging revealed significantly smaller tumors ($p < 0.05$) in *Ibsp* KO mice relative to WT controls (Figures

7C and 7D) indicating that endogenous Ibsp is important for GBM growth. To evaluate the potential role of *Ibsp* in migration, we examined the association of GFP-labeled tumor cells with lectin-labeled blood vessels located outside the main body of the tumor in *Ibsp* KO and WT mice. As shown in Figure 7E (highlighted by dashed white lines), glioma cells were more often found in close proximity to blood vessels in WT mice than in KO mice, highlighting the potential role of IBSP in promoting tumor cell invasion along vessels *in vivo*. Quantifying this effect, we found that the distance between GFP+ tumor cells and lectin+ blood vessels was significantly higher in *Ibsp* KO mice than in WT mice ($p = 0.025$, WT CI −0.57; −0.05, IBSP KO CI 0.09; 0.29) (Figure 7F) suggesting that *Ibsp* promotes growth and migration of tumor cells. Collectively, these findings indicate that vascular-derived IBSP plays an important role in growth and migration of GBM tumors.

DISCUSSION

Microvascular hyperproliferation is a major hallmark of GBM and a histopathological marker of poor prognosis (Das and Marsden, 2013). Prior studies demonstrated that the vasculature can provide a trophic niche that allows for the maintenance and survival of the adjacent glioma tumor cells (Calabrese et al., 2007; Jeon et al., 2014). For example, vascular cells support GBM stem-like cells in the face of radiation treatment (Garcia-Barros et al., 2003). Another important role for the vascular niche is in supporting migration out of the main body of the tumor and into the more normal parenchyma (Gilbertson and Rich, 2007; Griveau et al., 2018) sowing the seeds for tumor recurrence and disease relapse. The molecular mechanisms mediating these effects are only beginning to be understood.

Prior studies to delineate the genes enriched in GBM vasculature compared with low-grade tumors or normal brain have generally focused on the means by which the tumor induces the host vasculature to promote the genesis and ingrowth of hyperproliferative, abnormal vessels associated with GBM (Charalambous et al., 2005; Dieterich et al., 2012). The most important of these interactions include secretions of growth factors, such as VEGF and FGF, by tumor cells (Bao et al., 2006). There is ample evidence to consider the reverse signaling, where factors elaborated by the vasculature influence tumor biology. Here, we have utilized RNA sequencing and an informatics-based approach to delineate genes expressed by GBM vasculature, whose secreted extracellular factors are predicted to interact with proteins expressed by tumor cells. Our study is meant to provide a broader picture of the PVN-tumor interactome in order that other mechanisms can be targeted.

A key question to be asked is: Which interactome is most significant, one with a focus on those molecules enriched in both GBM vasculature and GTCs or one that is broader, taking into account all potential interactions? From a therapeutic perspective, there would be an inherent desirability to target pathways and factors that are enriched in GBM compared with normal brain. However, when considering the complete biology of the vascular-tumor interaction, proteins that are expressed by the glioma vasculature and the tumor cells, but not necessarily enriched compared with normal cells will still have the potential to play important roles in tumor progression. For this reason, we have described a more global interactome in addition to ones including only glioma-enriched genes.

One potential limitation of our study is in the choice of tumor and vascular cell populations. We selected the A2B5-expressing population because it has been demonstrated to encompass the glioma tumor-initiating cells (Auvergne et al., 2013; Ogden et al., 2008). Furthermore, this population can be compared directly to non-cancerous A2B5+ glial progenitors (Auvergne et al., 2013; Sun et al., 2015). In line with these studies, we found that this fraction expresses numerous genes in common with normal glial progenitors, but that it also has dysregulated oncogenic pathways, indicating that they are true cancer cells. However, it is possible that we have missed key tumor cells in our analysis that may not express A2B5. Similarly, we used CD31 to highly identify GVCs. However, it is likely that other cells that are tightly associated with endothelial cells, including pericytes and perivascular immune cells, are present within this fraction. Rather than considering such cells as “contaminants,” their lack of exclusion allows for the consideration of the vascular niche as-a-whole rather than on a cell-by-cell basis. Our comparison with single-cell analyses, which, in and of themselves are limited in depth, confirms the vascular expression of our genes of interest, including IBSP. Another potential limitation is our normal comparison sample. We utilized relatively normal regions from pediatric epilepsy tissue, as this was the most readily available source of fresh cells. It is possible that comparisons with vascular and A2B5-positive cells from the non-transformed white matter of tissue from an age group that fully overlapped with the one in which we isolated tumor and tumor vascular cells would yield somewhat different results.

Our informatics analysis provides strong support for the concept that a major role for the GBM vasculature is in the promotion of tumor cell migration. Pro-migratory functions dominated the gene ontologies of the interactome. *In vitro* analysis using a hydrogel-based co-culture system supports this hypothesis, as short-term, primary GVCs produce robust migration of cells out of GBM spheroid cultures. Our findings, however, do not preclude other roles for GVC-derived factors. Such roles could include effects on tumor cell survival and proliferation, with the latter function demonstrated for IBSP in this study. In addition, GVC-derived factors could play important roles and influence other cells in the tumor microenvironment, including immune cells.

As a proof of concept, we examined a relatively poorly studied protein, IBSP, and demonstrated its strong pro-migratory effects *in vitro* and *in vivo*. Given that there are numerous integrin-binding proteins associated with the tumor microenvironment, including other members of the SIBLING family, especially OPN (Lamour et al., 2015), we were surprised by the significance of IBSP, as knockdown of IBSP in GVCs appeared to completely abolish migration of tumor cells in our culture system, and tumors implanted into *Ibsp* KO mice showed a significantly reduced number of vascular-associated tumor cells outside the body of the tumor. A limitation of the latter finding is that, because we did not use cell-type-specific knockouts, we do not yet know which specific perivascular cells are responsible for regulating the association of the murine tumor cells with the vasculature. However, given that IBSP is associated with multiple cell types in the PVN, our use of the global knockout seems justified. It is important to note that our findings do not imply that IBSP is the only factor that regulates perivascular migration, as it seems likely that IBSP acts in concert with other factors. The mechanisms by which IBSP promotes GBM migration

remain to be fully elucidated, although it is clear that IBSP requires interaction with ITGαV for its pro-migration effect.

A somewhat surprising result was that, in addition to promoting migration, IBSP also promoted the proliferation of GBM cells, but that this effect, at least *in vitro*, was associated only with the proneural GBM lines tested. It is striking to note that IBSP expression is only associated with worse outcome in IDH-WT proneural GBM. The reasons why the *in vitro* pro-proliferative effects of IBSP are restricted to proneural cells are unknown. Cells of all three tumor subtypes express ITGαV and have a pro-migratory response to IBSP and, thus, it is not simply a matter of cells being insensitive to IBSP signaling. It is possible that the pro-proliferative response is due to action at other receptors or the activation of downstream pathways in proneural cells that are not activated in cells of the other two main subtypes, but the resolution of this question will require further study.

Our studies indicate that one potential therapeutic strategy could be selective targeting of the ITGαV on tumor cells to prevent tumor spread along the vasculature. However, we do not yet know whether such a strategy is feasible. Integrins play numerous roles in both glioma and normal brain biology and ITGαV is expressed by many cell types. Integrin blockade, particularly of αvβ3 and αvβ5 integrins with cilengitide has been attempted, but results have been disappointing (Khasraw et al., 2016; Stupp et al., 2014). We do not yet know whether an approach using a selective antibody, such as that used in the current study would be feasible, nor would it negate the potential for off-target effects based on ITGαV expression in other cell types within the brain.

In conclusion, our study utilized RNA sequencing, coupled with bioinformatics approaches, to describe a comprehensive GVC-GTC interactome. While we anticipate that the IBSP-ITGαV axis will be considered a target for therapeutic intervention, our elucidation of the broader GVC-GTC interactome is meant to serve as a resource for the brain tumor and, indeed, the cancer research community at large.

Limitations of the study

In addition to some of the limitations described above with respect to cell types of IBSP expression and the control samples employed, there are other limitations. Here, we utilized A2B5 to encompass glioma cells with stem cell-like potential. However, there is a likelihood that not all tumor cells are captured by this method and thus some tumor cells may behave differently than those we have isolated. Furthermore, while we have demonstrated that *Ibsp* is essential for tumor migration along the vessels using global *Ibsp* knockout mice, we have not clearly established that IBSP secreted by endogenous vessels is critical for promoting tumor migration, nor have we defined the function of the receptor ITGαV in mediating the effects of IBSP *in vivo*.

STAR★METHODS

RESOURCE AVAILABILITY

Lead contact—Any requests for resources and reagents should be directed to and will be fulfilled by the lead contact, Harley Kornblum (Hkornblum@mednet.ucla.edu).

Materials availability—This study did not generate new unique reagents.

Data and code availability

- All RNA-sequencing data have been deposited to GEO, and accession number is listed in the key resources table.
- This paper does not report any original code.
- Any additional information required to reanalyze the data in this paper will be available from the lead contact upon request.

EXPERIMENTAL MODEL AND SUBJECT DETAILS

Patient tissue samples—De-identified human tissue samples were obtained from surgical resections under an approved University of California, Los Angeles (UCLA) Institutional Review Board (IRB) protocol. Brain tumor samples were collected in collaboration with the UCLA Brain Tumor Translational Resource (BTTR) and were graded by the attending neuropathologist according to guidelines set forth by the World Health Organization (WHO). All tissues were collected with informed patient/guardian consent. Non-transformed samples were collected from children and adolescents (3–19 years old) and consist of small sections of healthy cortex or white matter, which were resected to gain access to deeper epileptic or otherwise pathological brain structures, and were considered normal according to MRI, and electroencephalogram studies (A). In total, we sequenced 7 primary GBM samples with no prior treatments, their GVC cell fractions, and from 5 of which we isolated the GTC cellular fractions (B). Samples from which specific cell types were isolated, were collected either in the operating room (non-transformed) or immediately following surgery through the pathologist, which allowed for a limited time (8–10 h) between tissue resection and our purification schemes. RNA extraction immediately followed cell type isolation, thus best representing the *in vivo* transcriptome of the cells, as acquired through RNA sequencing (RNA-seq). RNA-seq was also carried out on small pieces of un-dissociated parent GBMs and non-transformed gray matter (GM) and white matter (WM) as controls (B). Un-dissociated whole samples, i.e. GBM, and GM/WM, were stored in RNAlater (Thermo Fisher Scientific) at −20°C, or flash frozen immediately following resection, respectively. The un-dissociated samples were not used in downstream analyses and were only included as quality check controls.

Patient information—(A) Non-transformed samples, Primary Brain Glial Progenitor Cells (BGPC), Primary Brain Vascular cells (BVC), Gray Matter (GM), White Matter (WM).

Sample #	Cell fraction isolated for RNA-sequencing	Age	Gender	Surgical notes
12	BVC, BGPC	19	M	Left hemispherectomy for Left MCA perinatal stroke
13	BVC, BGPC	13	M	Left temporal occipital craniotomy for cortical dysplasia

Sample #	Cell fraction isolated for RNA-sequencing	Age	Gender	Surgical notes
14	GM and WM, BVC	5	F	Left frontal temporal craniotomy for resection of left cortical dysplasia.
15	GM and WM	12	F	Right hemispherectomy for diffuse right hemisphere cortical malformation and seizures with Lennox-Gastaut.
16	GM and WM	3	F	Right hemicraniotomy for epilepsy secondary to right intraventricular teratoma.

(B) GBM Tumor samples GBM Tumor Cells (GTC), GBM Vascular Cells (GVC).

Sample #	Diagnosis	Cell fraction isolated for RNA-sequencing	Age	Gender	Characteristics and cytogenetics TCGA classification
GBM4	GBM Primary with gigantocellular features	Unsorted, GVC	66	M	Maximum Ki67: 90%; MGMT Not Methylated; Multiple copies 7, 1,19. Monosomy 19. 10q loss **(subtype-indeterminant)**
GBM5	GBM, Primary with oligodendroglial component	Unsorted, GVC	42	M	Maximum Ki67: 70%; MGMT Methylated; IDH positive; Monosomy 10, **Proneural**
GBM6	GBM Primary	Unsorted, GVC, GTC	77	F	Maximum Ki67: 40%; MGMT Methylated; EGFR amplified, **Classical**
GBM7	GBM Primary	Unsorted, GVC, GTC	55	F	Maximum Ki67: 20%; MGMT Not Methylated; EGFR amplified; Monosomy 10, **Mesenchymal**
GBM8	GBM Primary	Unsorted, GVC, GTC	36	M	Maximum Ki67: 40%; EGFR amplified; Monosomy 10, **Subtype - indeterminant**
GBM9	GBM Primary	Unsorted, GVC, GTC	59	M	Maximum Ki67: 40%; MGMT Not Methylated; EGFR amplified; EGFR vIII positive, **Proneural**

Cell lines, culture and characterization.

Patient-derived GBM culture—GBM lines were established in our laboratory from patient tumor samples as gliomasphere cultures. Age, gender and patient characteristics were described previously (Laks et al., 2016). Gliomaspheres were cultured in DMEM/F12 medium supplemented with B27, 20 ng/ml bFGF, 50ng/ml EGF, 5μg/ml Heparin, and antibiotics pencillin/streptomycin. (Hemmati et al., 2003; Laks et al., 2009). Gliomaspheres were dissociated down to single cells with Accumax (Sigma) every 7–14 days depending on growth rate, and experiments were performed with lines that were cultured for <20 passages since their initial establishment, and tested negative for mycoplasma contamination.

GBM Lines	Age	Gender
HK_408	55	Female
HK_217	81	Male
HK_413	57	Female

GBM Lines	Age	Gender
HK_301	65	Male
HK_385	48	Male
HK_280	79	Male
HK_157	54	Female
HK_412	59	Female
HK_244	66	Female
HK_382	66	Male
HK_381	57	Female

Glioma vascular cell (GVC) culture—GVC (GVC15) line was generated from a recurrent GBM (Male, 65 years) patient tumor. Cells were cultured in endothelial growth media containing 2% FBS, 1% Penicillin-Streptomycin solution and growth supplement, and maintained for up to 5 passages from initial establishment. Characterization was performed by immunostaining using anti-human CD31 antibody at P1 and P3. DiI-Ac-LDL uptake assay was used to confirm the vascular characteristics of GVC. RNA-sequencing was performed at Passage 4 to characterize the GVC. FPKM values of vascular endothelial and pericyte markers are shown in55 the table in Figure S2D. **HEK293T cells** were obtained from ATCC and cultured in DMEM: F12 with 10% FBS and antibiotics.

Human brain microvascular endothelial cells—(HBMEC/BVC) were purchased from Sciencell and maintained in endothelial growth media.

Animal strains—The *Ibsp* knockout (ko) mice (129/svJ CD1 background) were a gift from Dr. Harvey Goldberg's laboratory at the University of Western Ontario. SCID mice were obtained from Jackson Laboratory. All animal experiments were carried out under an Institutional Animal Care and Use Committee (IACUC) approved protocol according to NIH guidelines at University of Alabama, Birmingham and University of California, Los Angeles.

***Ex vivo* IBSP treatment and generation of orthotopic tumor xenografts—**6–8 weeks old, female SCID mice were used to generate xenografts. Patient-derived GBM cell lines were pretreated for 3 days in synthetic IBSP or control peptide (IBSP-SCR); 10ug/ml; 0.33mM. On the day of injection, concentration of IBSP was increased 3x to 30ug/ml (1μM) in injection solution. 200,000 GBM cells were injected into the brains of SCID mice. Four weeks after injection, mice were sacrificed and perfused with ice-cold PBS and 4% (wt/vol) paraformaldehyde (PFA). Brains were dissected and fixed in 4% PFA for 24, hours and then transferred to 10% formalin, and sectioned for staining.

Murine GBM transplants in *Ibsp*^{wt} and *Ibsp*^{ko} mice—50,000 cells from a IDH-wildtype murine glioma line harboring NRAS-G12V,-TP53 -ATRX mutations (Nunez et al., 2019) containing firefly-luciferase-GFP was transplanted into equal numbers of male and female 8–12 weeks old *Ibsp* wt and ko mice. One week following transplantation, tumors were imaged for luciferase signal using IVIS Lumina II imager at the Crump Institute's

Preclinical Imaging Technology Center at UCLA. Briefly, animals were anesthetized with isoflurane and injected intraperitoneally with D-luciferin (100μL; GoldBio) dissolved in phosphate buffer saline without Ca^{2+} or Mg2+ (30 mg/mL). 4 min after injection animals were imaged on an IVIS Lumina II (Caliper Life Sciences. Bioluminescence images were overlaid on photographs of the mice using Living Image software (PerkinElmer) and ROIs were selected to encompass the tumor area and radiance was used as a measure of tumor burden.

METHOD DETAILS

Tumor tissue processing—To obtain a single cell suspension from the surgically resected tissues, samples (300–700 mg) were minced into ~1mm pieces, and incubated in 12500 U of Collagenase II and Collagenase IV in Hibernate A media at 37°C for 20 min with gentle agitation every 5min. Following enzymatic digestion, the cell suspension was passed through a 100μm filter and cells were pelleted at 1000×g for 5min. To remove cellular debris and red blood cells (RBC), the cell pellet was re-suspended in a total volume of 1.5ml of DMEM/F12, and 1.5ml of working 1X Percoll solution. RBCs were pelleted by centrifugation of this suspension at 1000×g for 5min. To the remaining supernatant and debris 1.5ml of 4X buffer was gradually added, to facilitate a shift in osmolality that would selectively allow live cells to pellet and centrifuged at 3000×g for 7min. Cells in the pellet were gradually re-introduced to normal salt concentrations by addition of 10–15ml media, were passed through a 40μm filter, and were again pelleted by centrifugation at 1000×g for 5min. The cells were then re-suspended in 1ml of phosphate buffered saline (PBS) containing 0.1% Bovine Serum Albumin and the number of cells and their viability were assessed.

Cell-type enrichment and purification by MACS and FACS—A vascular cell enrichment protocol was carried out using anti-human CD31 (PECAM-1) according to the manufacturer's protocol for positive selection of endothelial cells. From the EC-depleted fraction, A2B5+ cells were then isolated by FACS, as previously described (Auvergne et al., 2013). Briefly, cells were incubated in 500μl of A2B5 antibody supernatant for 30 min at 4°C. The cells were washed in 10mL of PBS and incubated in Alexa Fluor 488 Goat anti-mouse IgM secondary antibody (1:1000 in PBS with 0.5% BSA) for 30 min at 4°C. The cells were washed in 10mL of PBS, re-suspended at 1 million/ml in Hibernate A supplemented with B27, and stained with DAPI for dead cell exclusion, and 5μM DRAQ7 for nucleated cell inclusion. Depending on the quality of sample and extent of tissue necrosis, sorted A2B5+cells (DAPI−, DRAQ7+) ranged from 0.1%–2.3% of total cells. Appropriate isotype controls and un-stained cells were included, and cells were sorted on a FACS ARIA flow cytometer. Immediately following EC and A2B5+ cell preparation protocols, cells were lysed in 1mLl QIAzol lysis reagent. RNA isolation was carried out according to manufacturer's protocol RNA concentration and quality were assessed by NanoDrop spectrophotometer.

RNA sequencing and analysis—Total RNA integrity was examined using the Agilent Bioanalyzer 2000. 100ng of cDNA were used in the library preparation All samples were multiplexed into a single pool in order to avoid batch effects and sequenced using

an Illumina HiSeq 2000 sequencer. 45 million reads per sample were obtained, and quality control was performed on base qualities and nucleotide composition of sequences. Alignment to the H.sapiens (Hg38) refSeq reference gene annotation was performed using the STAR spliced read aligner with default parameters. Between 60 and 82% (avg 76%) of the reads mapped uniquely to the human genome. Total counts of read-fragments aligned to candidate gene regions were derived using HTSeq program (www.huber.embl.de/users/anders/HTSeq/doc/overview.html) with Human Hg38 refSeq as a reference and used as a basis for the quantification of gene expression. Only uniquely mapped reads were used for subsequent analyses. Differential expression analysis was conducted with R-project and the Bioconductor package edgeR. Statistical significance of the differential expression, expressed as Log_2 Fold Change (logFC), was determined, using tag-wise dispersion estimation, at p Value of <0.005 unless stated otherwise. FPKM values were reported as measure of relative expression units.

Ingenuity pathway analysis—IPA (www.ingenuity.com) was used in determining cellular localization of GTC/EC genes, and identifying direct and indirect protein interactions among EC extracellular factors and GTC PM molecules, along with manual curation and minimal use of the STRING functional protein association networks online tool (http://string-db.org), which was instrumental in developing the interactome (according to DEA, and the comprehensive interactome according to FPKM expression units). Canonical pathways, upstream regulators and disease and functions associated with a gene list were considered to be significant at $p < 0.05$ unless state otherwise. Circos plot was used to visualize the relationship between the plasma membrane interactors on GTC and secreted molecules on GVC in the interactome. Thickness of the arrows correspond to the FPKM values of the expression of ligands. R software and R packages dplyr, circlize, migest, randomcoloR were used for generating the Circos plot.

Analysis of single-cell RNA sequencing dataset—We utilized the single-cell RNA-sequencing data from CD31+ tumor endothelial cells isolated from core and edge regions of the primary GBM tumor samples from a previously published repository (Xie et al., 2021). Raw count matrices were downloaded from GEO and low quality cells that have mitochondrial or ribosomal reads more than 10% of total reads or have less than 200 features are excluded. Features not expressed in more than 5 cells were also excluded. Filtered count data were combined, and normalized using SCTransform. Data integration was performed using IntegrateData function in Seurat. Clusters were determined by shared nearest neighbor modularity optimization method. Cell types were determined by cell common type markers.

HA Thiolation—High molecular weight hyaluronic acid (HA) was thiolated according to established protocols (Xiao et al., 2018a). In all cases, molar ratios are reported with respect to HA carboxyl groups. Briefly, sodium hyaluronate (500–750 kDa, M_W = 700 kDa, Life core) was dissolved in deionized water (DI-H_2O). Next, 1-ethyl-3-[3-dimethylaminopropyl] carbodiimide (EDC, Thermofisher Scientific) was dissolved in DI-H_2O and added to the solution at a 0.25 molar ratio. N-hydroxysuccinimide (NHS, Acros Organics) was then added to the HA solution at a 0.125 molar ratio. The solution beaker was stirred

continuously at room temperature (RT) while pH was adjusted to 5.50 using 1 M HCl for 45 min. Then, cystamine dihydrochloride (Sigma-Aldrich) was added to the reaction at a molar ratio of 0.25 and pH was adjusted to 6.25 using 1 M NaOH. The reaction was continuously stirred at RT overnight. The next day, dithiothreitol (DTT, Sigma-Aldrich) was added (1 molar ratio), the solution pH adjusted to 8.50 using 1 M NaOH and the solution was stirred at RT for 2 h. The reaction was quenched by adjusting the pH to 4.0. The solution was then dialyzed (MWCO 14 kDa, regenerated cellulose, ThermoFisher Scientific) against pH 4.00 DI-H_2O for 3 days while protected from light. Dialysis water was refreshed twice daily. Purified HA was passed through 0.22 μm filters (EMD Millipore), flash frozen using liquid nitrogen and lyophilized. The dried product was vacuum sealed and stored at −20°C. Thiolation percentage was measured using ^{1}H-NMR spectroscopy and an Ellman's assay for free thiols.

Hydrogel fabrication and characterization—Hydrogel precursor solution was prepared by dissolving HA-SH (0.5% w/v), 4-arm thiol terminated polyethylene glycol (PEG-SH) (Laysan Bio), 8-arm norbornene terminated polyethylene glycol (PEG-Norb) (Jenkem), 0.025% w/v lithium phenyl-2,4,6 trimethylben-zoylphosphinate (LAP, Sigma-Aldrich) and 0.25 mM thiolated peptides (RGD: GCGYGRGDSPG; IBSP: GCGYGGGGNGEPRGD NYRAY; JenKem, USA) in 20 mM HEPES buffer (pH = 7). The hydrogel precursor solution was cast into 8 mm diameter silicone rubber molds (Grace Biolabs) and irradiated with long-wave UV (365 nm, 4.2 mW/cm^2) (Blak-Ray B-100A UV lamp, UVP™) for 15 s. Hydrogel storage moduli (G′) were measured using a discovery hybrid rheometer-2 (DHR-2, TA Instruments) at 37°C. Frequency sweeps were performed under 1% constant strain in the range of 0.1–1.0 Hz. Storage modulus of each sample was calculated as the average value of the linear region of the storage curve from the frequency sweep plot. For statistical analysis, 3 separate measurements were taken in which 5 samples from each condition were measured.

GBM encapsulation in hydrogels—Patient-derived GBM cell lines, HK217 (proneural), HK301 (proneural) and HK280 (mesenchymal) were used for encapsulation. Sizes of GBM spheroids were standardized by seeding approximately 600K cells per well into Aggrewell™ well plates (Stemcell Technologies) one day prior to encapsulation. The following day, spheroids were harvested from the wells, centrifuged briefly (200×G, 1 min) and resuspended in the hydrogel precursor solution. Spheroid-laden hydrogels were formed as described in the above hydrogel fabrication section. Cell migration was observed periodically (Imaged at Day 1,3,6 and 9) by acquiring phase contrast images on a Zeiss Axio.Z1 Observer microscope with a Hamamatsu Orca Flash 4.0 V2 Digital CMOS Camera and Zeiss ZEN 2 (Blue Edition) software. Quantitation is described separately. At the end of experimental period, hydrogels were fixed using 4% paraformaldehyde (PFA) and stained with Hoescht (nuclei) and Cell Mask™ (cell membrane). These gels were imaged using a Leica SP5 confocal microscope. To block ITGαV-IBSP interaction, GBM spheroids were incubated with 10 μg/mL anti-ITGαV antibody a day prior to encapsulation. In addition, after the encapsulation, hydrogels were incubated in GBM media containing 10 μg/mL of the same antibody over the course of the experiment.

GBM-GVC co-encapsulation—Human brain microvascular endothelial cells (HBEC) and GVC were cultured using endothelial cell media. GBM cells were infected with a lentivial vector encoding for blue fluorescent protein (BFP) to distinguish them from GVC which were infected with mCherry. We used the Aggrewell™ (above) to obtain spheroids of relatively uniform sizes. Co-cultures of GVC and GBM cells were established in two steps. First, GBM spheroids were resuspended in HA hydrogel precursor, casted in 4 mm diameter, silicone rubber molds and hydrogels crosslinked as described above. In the second step, GBM spheroid-laden hydrogels were transferred into 8 mm diameter molds and solution of HA-RGD (500μM RGD) containing GVC (10^7 cell/ml) was casted around the initial hydrogel and formed under UV. Final hydrogels were transferred to EC medium and imaged periodically (timepoints similar to previous part) as described above. At the end of experiments (Day 9), hydrogels were fixed using 4% PFA and imaged using a Leica SP5 confocal microscope.

Migration analysis in hydrogels—Cell migration was quantified using shape factor (circularity) and length of migration from sphere edge. To calculate circularity, perimeter of each sphere was marked in ImageJ software and circularity ($4\pi A/P^2$, A = area, P = perimeter) was calculated using ImageJ shape description. Briefly, using the free drawing tool, we traced the periphery of spheres and then calculate the shape factor using shape description analysis in ImageJ. Shape factor is defined as $4\pi A/P^2$, where A is the area and P is the perimeter of a spheroids. Shape factor values in general range from 0 to 1 in which 1 means complete circle and values smaller than 1 means deviation from a circle. With this method, more migratory spheres have shape factor values close to 0. As an arbitrary measurement, based on our data, we categorized migration in to 1) non-migratory: shape factor 1–0.7, 2) mild migration: shape factor 0.7–0.3 and 3) invasive: shape factor <0.3. We measured shape factor for 10 spheres per group from 3 independent experiments. For average migration distance, we used the line measurement option in ImageJ and measured the length of migratory processes from the sphere periphery for 10 GBM spheroids and 3 independent experiments.

Immunohistochemistry—Formalin fixed paraffin embedded (FFPE) patient GBM tissue blocks and tumor sections from mouse xenografts were sectioned at a thickness at 10μm and 5μm respectively. Antigen retrieval was performed on deparaffinized and rehydrated sections with 0.1M sodium citrate, pH 6.1 and pepsin-mediated antigen retrieval. Endogenous peroxidase activity was quenched in 0.3% H_2O_2 in TBS. Sections were incubated in blocking solution (5% Normal Goat or Donkey serum and 1% BSA in TBST). Appropriate primary antibodies were added and incubated overnight at 4°C in a humidified chamber. Biotinylated secondary antibody, and HRP-antibody were added and incubated at RT. DAB kit was used to visualize the antibody staining and hematoxylin was used as nuclear counter stain. DAB stained images were obtained using EVOS FL Auto Imaging System. Quantitation of percentage of DAB + are per image was measured using ImageJ. For **immunofluorescence staining**, cells were fixed with 4% Paraformaldehyde for 15 min. Cells were washed with PBS and incubated in blocking solution (2% BSA in PBS). Appropriate primary antibodies were added and incubated overnight at 4°C in a humidified chamber. Cells were incubated with species-appropriate goat/donkey secondary antibodies

coupled to AlexaFluor dyes (568, Invitrogen) and Hoechst dye for nuclear staining for 2 h at RT. Imaging was performed using Leica LAS X or EVOS FL Auto Imaging System.

Microarray-based gene expression analysis—Concentration and quality of RNA samples were examined using the NanoDrop ND-1000 Spectrophotometer (NanoDrop Technologies) and the Agilent 2100 Bioanalyzer (Agilent Technologies). RNA samples were reverse transcribed and labeled according to the manufacturer's instructions and hybridized to Affymetrix high-density oligonucleotide HG-U133A Plus 2.0 Human Arrays. Microarray data analysis was performed as described previously. Briefly, array preprocessing was completed in the R computing environment (http://www.r-project.org) using Bioconductor packages (http://www.bioconductor.org). Raw data were normalized using the robust multiarray method (12582260). To eliminate batch effects, additional normalization was performed using the R package "ComBat" (http://statistics.byu.edu/johnson/ComBat; 16632515) with default parameters. Contrast analysis of differential expression was performed using the LIMMA package. After linear model fitting, a Bayesian estimate of differential expression was calculated using a modified t test. The threshold for statistical significance was set at $p < 0.005$ for differential expression analysis and $p < 0.01$ for explorative analyses (gene ontology and pathway analysis). Gene ontology and pathway analysis were carried out using the Database for Annotation, Visualization and Integrated Discovery (DAVID, https://david.ncifcrf.gov), GSEA (16199517), and Ingenuity Pathway Analysis (IPA; www.ingenuity.com).

TCGA gliomasphere classification—Our gliomasphere transcriptomes were classified into the three (Classical, Mes, and PN) clinically relevant TCGA sub-classifications as previous described (Laks et al., 2016). Briefly, the 173 core TCGA glioblastoma samples used in TCGA subclassifications of GBMs (Verhaak et al., 2010) were used to build our classification model. The TCGA unified gene expression data (across three microarray platforms: Affymetrix HuEx array, Affymetrix U133A array and Agilent 244K) were combined with our gliomasphere data from Affymetrix U133 plus 2.0 array, and utilizing the limma R package, they were normalized together (Smyth et al., 2005). Following batch effect normalization using the ComBat R package (http://statistics.byu.edu/johnson/ComBat/).

(Johnson et al., 2007), we used the LDA based centroid classification algorism (ClaNC) used by (Verhaak et al., 2010) to develop a 3-class centroid-based classifier from 38 Classical, 56 Mes, and 53 PN TCGA samples (Dabney, 2006), where the 26 TCGA neural samples were excluded. Only 789 of the of the 840 TCGA classifier genes were used to assign classifications to our gliomaspheres, due to limitations in gene name overlap between TCGA and our platforms.

shRNA screening—shRNA clones of the genes of interest were arrayed from our genome wide shRNA library (Silva et al., 2005). *100 ng shRNA encoding pGIPZ plasmid was spotted into PDL coated 96 well plates and 100 ng pCMVd8.91 with 10 ngpMD2G was added together with Mirus TransIT in a 1:3 ratio and incubated for 20 min in a total volume of 25 μL. 75 μL containing 40,000 293T cells were added on top to a total of 100 μL in DMEM with 30% FBS with 1x PSG, NEN and HEPES. Successful transfection was*

confirmed after 24 h at 37°C and 5% C O 2 by GFP expression of the cells. Virus was harvested after 48 h at 37°C and 5% C O 2 and 7.5 μL virus containing media was plated into each well of a 384 well plate using an Agilent Vprep in a custom HEPA filtered enclosure. Media was added to 25μL total volume before cells were added at [100000/mL], to a total of 50ul volume/well. 3 days post-transduction, small GBM spheroids were encapsulated in hydrogels plated in another 384-well plate.

High-throughput imaging and quantification of gliomasphere migration— Gliomaspheres were encapsulated in hydrogels and plated in 384-well Greiner plates and imaged using a Molecular Devices ImageXpress XL platform. In short, plates were imaged using a Nikon 10x objective (0.3NA, Plan Apo) with no binning and laser auto-focusing. Plates were imaged daily, and were treated with Hoechst, at 1:3000 in media, overnight before the final imaging that were to be used for quantification. The resulting images were analyzed using the MetaXpress Custom Module editor. A custom module was set up using Adaptive Thresholding in the UV/DAPI channel with a size window from 10 to 400 micron and an intensity over local background of at least 1750 gray scales. This analysis applied a mask to the images, thus allowing for quantification of the number of objects dispersed within the hydrogel. Though this method of quantification is an underestimation of the number of cells, it does provide for an efficient means to quantify dispersion from the gliomasphere core for our HT purposes. The following parameters were extracted on an object by object base: Total area average, area average per object, centroid position for x and y axis. Also, the sums for the same parameters were extracted. The Elledge form factor was extracted on an object by object base.

Fluorescent *in situ* hybridization by RNAScope—FFPE tumor sections were baked at 60°C for 1 h, then deparaffinized with xylene and rehydrated in a series of washes with decreasing ethanol concentrations. Antigen retrieval and *in situ* hybridization was performed according to the protocol for the RNAScope™ Fluorescent Multiplex Assay (ACDBio). Targets were labelled with Cy3-and Cy5-tyramide TSA solutions (1:700, Perkin Elmer) and coverslips mounted with Prolong Gold Mounting Medium with DAPI.

Quantitative RT-PCR—RNA was isolated with RNeasy Micro or Mini Kit (QIAGEN), and 500–1000ng of RNA was used for first-strand cDNA synthesis using random primers and Superscript Reverse Transcriptase (Invitrogen). qRT–PCR was performed using Power SYBR Green PCR Master Mix (Applied Biosystems). The relative expression of genes was normalized using 18srRNA as the housekeeping gene. All experiments were repeated at least 3 times, and data are represented as mean ± SD. Primers are listed in Table S6.

Cell proliferation assay—The Cell Counting Kit-8 (Dojindo Molecular Technologies Inc.) and CellTiter-Glo Luminescent cell viability assay (Promega) was used according to the manufacturer's protocol. Freshly dissociated gliomaspheres were plated at 5000cells/100μL/well in a 96-well plate and allowed to proliferated for either 3 or 7 days at which point cell numbers of the experimental conditions (250nM IBSP in all cases unless specified otherwise) were assessed as compared to control (CTRL) conditions. Luminescence signal for CellTiter-Glo asay was measured in a luminometer, and readings

were taken on Day 0 of plating and at Day 3 after treatment to normalize for plating density and obtain fold change in growth of cells.

Western blot—Protein lysates were obtained from 300k cells per sample using RIPA buffer supplemented with protease and phosphatase inhibitors. To prepare Western blot samples, protein solutions were mixed with Laemmli buffer (2X, contain 5 %v/v β-mercapto ethanol, bio-rad) in 1:1 ratio and heated at 97°C for 5 min. Samples were loaded in a Nupage™ 4–12% bis-Tris protein gel (Thermoscientific). Gels were run in MOPS-SDS buffer (20X, thermo fisher) at 60V for 15 min the 165V for 1 h. Later proteins were transferred onto a PVDF membrane (Thermo Scientific™) in tris/glycine (10X, Bio-Rad) buffer containing 20 %v/v methanol. IBSP detection was done using a human IBSP polycolonal antibody (Rabbit, Thermo Fisher Scientific) as the primary antibody and then a goat anti-rabbit IgG (HRP linked, cell signaling). For the housekeeping gene, GAPDH was stained using a GAPDH loading control antibody (mouse, Fisher Scientific) and then a goat anti-mouse IgG secondary antibody (HRP, Novus biological). Protein bands were developed using the Clarity™ western ECL substrate (Bio-Rad). Protein bands were visualized using MYECL gel imager (Thermo Scientific). Quantification of protein levels were done in ImageJ.

Tumor cell-blood vessel distance quantification—30μm thick cryosectioned tissue sections containing GFP-expressing tumors were stained with Hoechst nuclear stain (Millipore Sigma) and DyLight 649-conjugated tomato lectin dye (Vector Labs) to label blood vessels. Images were acquired on an AxioImager.M2 (Zeiss) equipped with an Apotome 2. Pseudoconfocal z-stacks were taken to envelope the depth of the tissue section and a maximum intensity projection was used for quantification. File names were de-identified and randomized for ImageJ analysis by blind observers. A border was drawn around the main tumor and only cells outside the border were counted and measured. Distance in μm between GFP-expressing tumor cells and nearest lectin-stained blood vessel were measured using the line tool. Data are represented as boxplots of individual cell-blood vessel measurements for each animal.

QUANTIFICATION AND STATISTICAL ANALYSIS

Graphpad Prism 9 was used for statistical tests and details can be found in figure legends. All *in vitro* experiments were done with at least three technical replicates and repeated in multiple independent experiments. Error bars on all the graphs show Mean and Standard deviation (SD) unless specified otherwise. Small group comparisons were done using the Student's t-test and $p < 0.05$ was deemed significant. Gene expression and correlation statistical analysis methods are described above. For gliomasphere migration in HA-3D culture systems, normality of each dataset was analyzed using D'Agostino & Pearson omnibus normality test. For normally distributed population, one-way ANOVA followed by post-hoc t test were used to determine the statistical differences among the groups.

Supplementary Material

Refer to Web version on PubMed Central for supplementary material.

ACKNOWLEDGMENTS

The authors thank the UCLA BTTR and Dr. William Yong, UNGC, JCCC Flow Cytometry Core, UCLA Broad Stem Cell Research Center, Dr. Xinmin Li, and the UCLA Clinical Microarray Core for technical contributions. We thank Dr. Robert Damoiseaux and the UCLA Molecular Screening Shared Resource for assistance with shRNA screening. We thank Holly Wilhalme in the UCLA Institute for Digital Research and Education (IDRE) for aid in figure presentation. The IBSP knockout mice were generously supplied by Drs. Martha Somerman and Harvey Goldberg at the National Institute of Arthritis and Musculoskeletal and Skin Diseases. The murine glioma line was a kind gift from Drs. Maria Castro and Pedro Lowenstein. This work was supported by grants from the Dr. Miriam and Sheldon G. Adelson Medical Research Foundation (to S.A.G., S.T.C., and H.I.K.), The National Institutes of Health grants P50 CA211015 (to L.L. and H.I.K.), CA241927–01A1 (to S.K.S. and H.I.K.) and CA197943 (to M.L.I-A.), and RO1 NS121617 (to H.I.K.) and RO1 NS112256 (to S.T.C.). This work was also supported by a University of California Cancer Research Coordinating Committee Award, a Broad Stem Cell Research Center Seed Grant, and an American Brain Tumor Association Discovery Award (to S.K.S.).

REFERENCES

Auvergne RM, Sim FJ, Wang S, Chandler-Militello D, Burch J, Al Fanek Y, Davis D, Benraiss A, Walter K, Achanta P, et al. (2013). Transcriptional differences between normal and glioma-derived glial progenitor cells identify a core set of dysregulated genes. Cell Rep. 3, 2127–2141. 10.1016/j.celrep.2013.04.035. [PubMed: 23727239]

Bao S, Wu Q, Sathornsumetee S, Hao Y, Li Z, Hjelmeland AB, Shi Q, McLendon RE, Bigner DD, and Rich JN (2006). Stem cell-like glioma cells promote tumor angiogenesis through vascular endothelial growth factor. Cancer Res. 66, 7843–7848. 10.1158/0008-5472.CAN-06-1010. [PubMed: 16912155]

Bellahcène A, Castronovo V, Ogbureke KUE, Fisher LW, and Fedarko NS (2008). Small integrin-binding ligand N-linked glycoproteins (SIBLINGs): multifunctional proteins in cancer. Nat. Rev. Cancer 8, 212–226. 10.1038/nrc2345. [PubMed: 18292776]

Bowman RL, Wang Q, Carro A, Verhaak RGW, and Squatrito M (2017). GlioVis data portal for visualization and analysis of brain tumor expression datasets. Neuro Oncol. 19, 139–141. 10.1093/neuonc/now247. [PubMed: 28031383]

Brat DJ, and Van Meir EG (2001). Glomeruloid microvascular proliferation orchestrated by VPF/VEGF: a new world of angiogenesis research. Am. J. Pathol. 158, 789–796. 10.1016/S0002-9440(10)64025-4. [PubMed: 11238026]

Brooks LJ, and Parrinello S (2017). Vascular regulation of glioma stem-like cells: a balancing act. Curr. Opin. Neurobiol. 47, 8–15. 10.1016/j.conb.2017.06.008. [PubMed: 28732340]

Calabrese C, Poppleton H, Kocak M, Hogg TL, Fuller C, Hamner B, Oh EY, Gaber MW, Finklestein D, Allen M, et al. (2007). A perivascular niche for brain tumor stem cells. Cancer Cell 11, 69–82. 10.1016/j.ccr.2006.11.020. [PubMed: 17222791]

Charalambous C, Hofman FM, and Chen TC (2005). Functional and phenotypic differences between glioblastoma multiforme-derived and normal human brain endothelial cells. J. Neurosurg. 102, 699–705. 10.3171/jns.2005.102.4.0699. [PubMed: 15871513]

Charalambous C, Virrey J, Kardosh A, Jabbour MN, Qazi-Abdullah L, Pen L, Zidovetzki R, Schönthal AH, Chen TC, and Hofman FM (2007). Glioma-associated endothelial cells show evidence of replicative senescence. Exp. Cell Res. 313, 1192–1202. 10.1016/j.yexcr.2006.12.027. [PubMed: 17291495]

Charles N, and Holland EC (2010). The perivascular niche microenvironment in brain tumor progression. Cell Cycle 9, 3012–3021. 10.4161/cc.9.15.12710. [PubMed: 20714216]

Charles N, Ozawa T, Squatrito M, Bleau A-M, Brennan CW, Hambardzumyan D, and Holland EC (2010). Perivascular nitric oxide activates notch signaling and promotes stem-like character in PDGF-induced glioma cells. Cell Stem Cell 6, 141–152. 10.1016/j.stem.2010.01.001. [PubMed: 20144787]

Dabney AR (2006). ClaNC: point-and-click software for classifying microarrays to nearest centroids. Bioinformatics 22, 122–123. 10.1093/bioinformatics/bti756. [PubMed: 16269418]

Das S, and Marsden PA (2013). Angiogenesis in glioblastoma. N. Engl. J. Med. 369, 1561–1563. 10.1056/NEJMcibr1309402. [PubMed: 24131182]

Dieterich LC, Mellberg S, Langenkamp E, Zhang L, Zieba A, Salomäki H, Teichert M, Huang H, Edqvist P-H, Kraus T, et al. (2012). Transcriptional profiling of human glioblastoma vessels indicates a key role of VEGF-A and TGFβ2 in vascular abnormalization. J. Pathol. 228, 378–390. 10.1002/path.4072. [PubMed: 22786655]

Farin A, Suzuki SO, Weiker M, Goldman JE, Bruce JN, and Canoll P (2006). Transplanted glioma cells migrate and proliferate on host brain vasculature: a dynamic analysis. Glia 53, 799–808. 10.1002/glia.20334. [PubMed: 16541395]

Garcia-Barros M, Paris F, Cordon-Cardo C, Lyden D, Rafii S, Haimovitz-Friedman A, Fuks Z, and Kolesnick R (2003). Tumor response to radiotherapy regulated by endothelial cell apoptosis. Science 300, 1155–1159. 10.1126/science.1082504. [PubMed: 12750523]

Gilbertson RJ, and Rich JN (2007). Making a tumour's bed: glioblastoma stem cells and the vascular niche. Nat. Rev. Cancer 7, 733–736. 10.1038/nrc2246. [PubMed: 17882276]

Griveau A, Seano G, Shelton SJ, Kupp R, Jahangiri A, Obernier K, Krishnan S, Lindberg OR, Yuen TJ, Tien A-C, et al. (2018). A glial signature and Wnt7 signaling regulate glioma-vascular interactions and tumor microenvironment. Cancer Cell 33, 874–889.e7. 10.1016/j.ccell.2018.03.020. [PubMed: 29681511]

Hemmati HD, Nakano I, Lazareff JA, Masterman-Smith M, Geschwind DH, Bronner-Fraser M, and Kornblum HI (2003). Cancerous stem cells can arise from pediatric brain tumors. Proc. Natl. Acad. Sci. USA 100, 15178–15183. 10.1073/pnas.2036535100. [PubMed: 14645703]

Jeon H-M, Kim S-H, Jin X, Park JB, Kim SH, Joshi K, Nakano I, and Kim H (2014). Crosstalk between glioma-initiating cells and endothelial cells drives tumor progression. Cancer Res. 74, 4482–4492. 10.1158/0008-5472.CAN-13-1597. [PubMed: 24962027]

Johnson WE, Li C, and Rabinovic A (2007). Adjusting batch effects in microarray expression data using empirical Bayes methods. Biostatistics 8, 118–127. 10.1093/biostatistics/kxj037. [PubMed: 16632515]

Karadag A, Ogbureke KUE, Fedarko NS, and Fisher LW (2004). Bone sialoprotein, matrix metalloproteinase 2, and alpha(v)beta3 integrin in osteotropic cancer cell invasion. J. Natl. Cancer Inst. 96, 956–965. 10.1093/jnci/djh169. [PubMed: 15199115]

Khasraw M, Lee A, McCowatt S, Kerestes Z, Buyse ME, Back M, Kichenadasse G, Ackland S, and Wheeler H (2016). Cilengitide with metronomic temozolomide, procarbazine, and standard radiotherapy in patients with glioblastoma and unmethylated MGMT gene promoter in ExCentric, an open-label phase II trial. J. Neuro Oncol. 128, 163–171. 10.1007/s11060-016-2094-0.

Krishnan S, Szabo E, Burghardt I, Frei K, Tabatabai G, and Weller M (2015). Modulation of cerebral endothelial cell function by TGF-β in glioblastoma: VEGF-dependent angiogenesis versus endothelial mesenchymal transition. Oncotarget 6, 22480–22495. 10.18632/oncotarget.4310. [PubMed: 26090865]

Laks DR, Masterman-Smith M, Visnyei K, Angenieux B, Orozco NM, Foran I, Yong WH, Vinters HV, Liau LM, Lazareff JA, et al. (2009). Neurosphere formation is an independent predictor of clinical outcome in malignant glioma. Stem Cell. 27, 980–987. 10.1002/stem.15.

Laks DR, Crisman TJ, Shih MYS, Mottahedeh J, Gao F, Sperry J, Garrett MC, Yong WH, Cloughesy TF, Liau LM, et al. (2016). Largescale assessment of the gliomasphere model system. Neuro Oncol. 18, 1367–1378. 10.1093/neuonc/now045. [PubMed: 27116978]

Lamour V, Henry A, Kroonen J, Nokin M-J, von Marschall Z, Fisher LW, Chau T-L, Chariot A, Sanson M, Delattre J-Y, et al. (2015). Targeting osteopontin suppresses glioblastoma stem-like cell character and tumorigenicity in vivo. Int. J. Cancer 137, 1047–1057. 10.1002/ijc.29454. [PubMed: 25620078]

Malaval L, Wade-Guéye NM, Boudiffa M, Fei J, Zirngibl R, Chen F, Laroche N, Roux J-P, Burt-Pichat B, Duboeuf F, et al. (2008). Bone sialoprotein plays a functional role in bone formation and osteoclastogenesis. J. Exp. Med. 205, 1145–1153. 10.1084/jem.20071294. [PubMed: 18458111]

Musumeci G, Castorina A, Magro G, Cardile V, Castorina S, and Ribatti D (2015). Enhanced expression of CD31/platelet endothelial cell adhesion molecule 1 (PECAM1) correlates with hypoxia inducible factor-1 alpha (HIF-1α) in human glioblastoma multiforme. Exp. Cell Res. 339, 407–416. 10.1016/j.yexcr.2015.09.007. [PubMed: 26376118]

Núñez FJ, Mendez FM, Kadiyala P, Alghamri MS, Savelieff MG, Garcia-Fabiani MB, Haase S, Koschmann C, Calinescu A-A, Kamran N, et al. (2019). IDH-R132H acts as a tumor suppressor in glioma via epigenetic up-regulation of the DNA damage response. Sci. Transl. Med. 11, eaaq1427. 10.1126/scitranslmed.aaq1427. [PubMed: 30760578]

Ogden AT, Waziri AE, Lochhead RA, Fusco D, Lopez K, Ellis JA, Kang J, Assanah M, McKhann GM, Sisti MB, et al. (2008). Identification of A2B5+CD133− tumor-initiating cells in adult human gliomas. Neurosurgery 62, 505–514. 10.1227/01.neu.0000316019.28421.95. [PubMed: 18382330]

Pen A, Moreno MJ, Martin J, and Stanimirovic DB (2007). Molecular markers of extracellular matrix remodeling in glioblastoma vessels: microarray study of laser-captured glioblastoma vessels. Glia 55, 559–572. 10.1002/glia.20481. [PubMed: 17266141]

Scholz A, Harter PN, Cremer S, Yalcin BH, Gurnik S, Yamaji M, Di Tacchio M, Sommer K, Baumgarten P, Bähr O, et al. (2016). Endothelial cell-derived angiopoietin-2 is a therapeutic target in treatment-naive and bevacizumab-resistant glioblastoma. EMBO Mol. Med. 8, 39–57. 10.15252/emmm.201505505. [PubMed: 26666269]

Silva JM, Li MZ, Chang K, Ge W, Golding MC, Rickles RJ, Siolas D, Hu G, Paddison PJ, Schlabach MR, et al. (2005). Second-generation shRNA libraries covering the mouse and human genomes. Nat Genet 37, 1281–1288. 10.1038/ng1650. [PubMed: 16200065]

Smyth GK, Michaud J, and Scott HS (2005). Use of within-array replicate spots for assessing differential expression in microarray experiments. Bioinformatics 21, 2067–2075. 10.1093/bioinformatics/bti270. [PubMed: 15657102]

Stratmann A, Risau W, and Plate KH (1998). Cell type-specific expression of angiopoietin-1 and angiopoietin-2 suggests a role in glioblastoma angiogenesis. Am. J. Pathol. 153, 1459–1466. 10.1016/S0002-9440(10)65733-1. [PubMed: 9811337]

Stupp R, Hegi ME, Gorlia T, Erridge SC, Perry J, Hong Y-K, Aldape KD, Lhermitte B, Pietsch T, Grujicic D, et al. (2014). Cilengitide combined with standard treatment for patients with newly diagnosed glioblastoma with methylated MGMT promoter (CENTRIC EORTC 26071–22072 study): a multicentre, randomised, open-label, phase 3 trial. Lancet Oncol. 15, 1100–1108. 10.1016/S1470-2045(14)70379-1. [PubMed: 25163906]

Stupp R, Taillibert S, Kanner AA, Kesari S, Steinberg DM, Toms SA, Taylor LP, Lieberman F, Silvani A, Fink KL, et al. (2015). Maintenance Therapy With Tumor-Treating Fields Plus Temozolomide vs Temozolomide Alone for Glioblastoma: A Randomized Clinical Trial. JAMA 314, 2535–2543. 10.1001/jama.2015.16669. [PubMed: 26670971]

Sun T, Chen G, Li Y, Xie X, Zhou Y, and DU Z (2015). Aggressive invasion is observed in CD133(−)/A2B5(+) glioma-initiating cells. Oncol. Lett. 10, 3399–3406. 10.3892/ol.2015.3823. [PubMed: 26788141]

Sung V, Stubbs JT, Fisher L, Aaron AD, and Thompson EW (1998). Bone sialoprotein supports breast cancer cell adhesion proliferation and migration through differential usage of the alpha(v)beta3 and alpha(v)beta5 integrins. J. Cell. Physiol. 176, 482–494. 10.1002/(SICI)1097-4652. [PubMed: 9699501]

Tchoghandjian A, Baeza N, Colin C, Cayre M, Metellus P, Beclin C, Ouafik L, and Figarella-Branger D (2010). A2B5 cells from human glioblastoma have cancer stem cell properties. Brain Pathol. 20, 211–221. 10.1111/j.1750-3639.2009.00269.x. [PubMed: 19243384]

Verhaak RGW, Hoadley KA, Purdom E, Wang V, Qi Y, Wilkerson MD, Miller CR, Ding L, Golub T, Mesirov JP, et al. (2010). Integrated genomic analysis identifies clinically relevant subtypes of glioblastoma characterized by abnormalities in PDGFRA, IDH1, EGFR, and NF1. Cancer Cell 17, 98–110. 10.1016/j.ccr.2009.12.020. [PubMed: 20129251]

Xiao W, Zhang R, Sohrabi A, Ehsanipour A, Sun S, Liang J, Walthers CM, Ta L, Nathanson DA, and Seidlits SK (2018a). Brain-mimetic 3D culture platforms allow investigation of Cooperative effects of extracellular matrix features on therapeutic resistance in glioblastoma. Cancer Res. 78, 1358–1370. 10.1158/0008-5472.CAN-17-2429. [PubMed: 29282221]

Xiao W, Ehsanipour A, Sohrabi A, and Seidlits SK (2018b). Hyaluronicacid based hydrogels for 3-Dimensional culture of patient-derived glioblastoma cells. J. Vis. Exp, e58176. 10.3791/58176.

Xiao W, Wang S, Zhang R, Sohrabi A, Yu Q, Liu S, Ehsanipour A, Liang J, Bierman RD, Nathanson DA, and Seidlits SK (2020). Bioengineered scaffolds for 3D culture demonstrate extracellular

matrix-mediated mechanisms of chemotherapy resistance in glioblastoma. Matrix Biol. 85–86, 128–146. 10.1016/j.matbio.2019.04.003.

Xie Y, He L, Lugano R, Zhang Y, Cao H, He Q, Chao M, Liu B, Cao Q, Wang J, et al. (2021). Key molecular alterations in endothelial cells in human glioblastoma uncovered through single-cell RNA sequencing. JCI Insight 6, 150861. 10.1172/jci.insight.150861. [PubMed: 34228647]

Yan G-N, Yang L, Lv Y-F, Shi Y, Shen L-L, Yao X-H, Guo Q-N, Zhang P, Cui Y-H, Zhang X, et al. (2014). Endothelial cells promote stem-like phenotype of glioma cells through activating the Hedgehog pathway. J. Pathol. 234, 11–22. 10.1002/path.4349. [PubMed: 24604164]

Highlights

- A molecular interactome of GBM tumor and vascular cells
- Vascular cells promote GBM migration in 3D hydrogels
- IBSP is a perivascular niche factor that promotes GBM migration

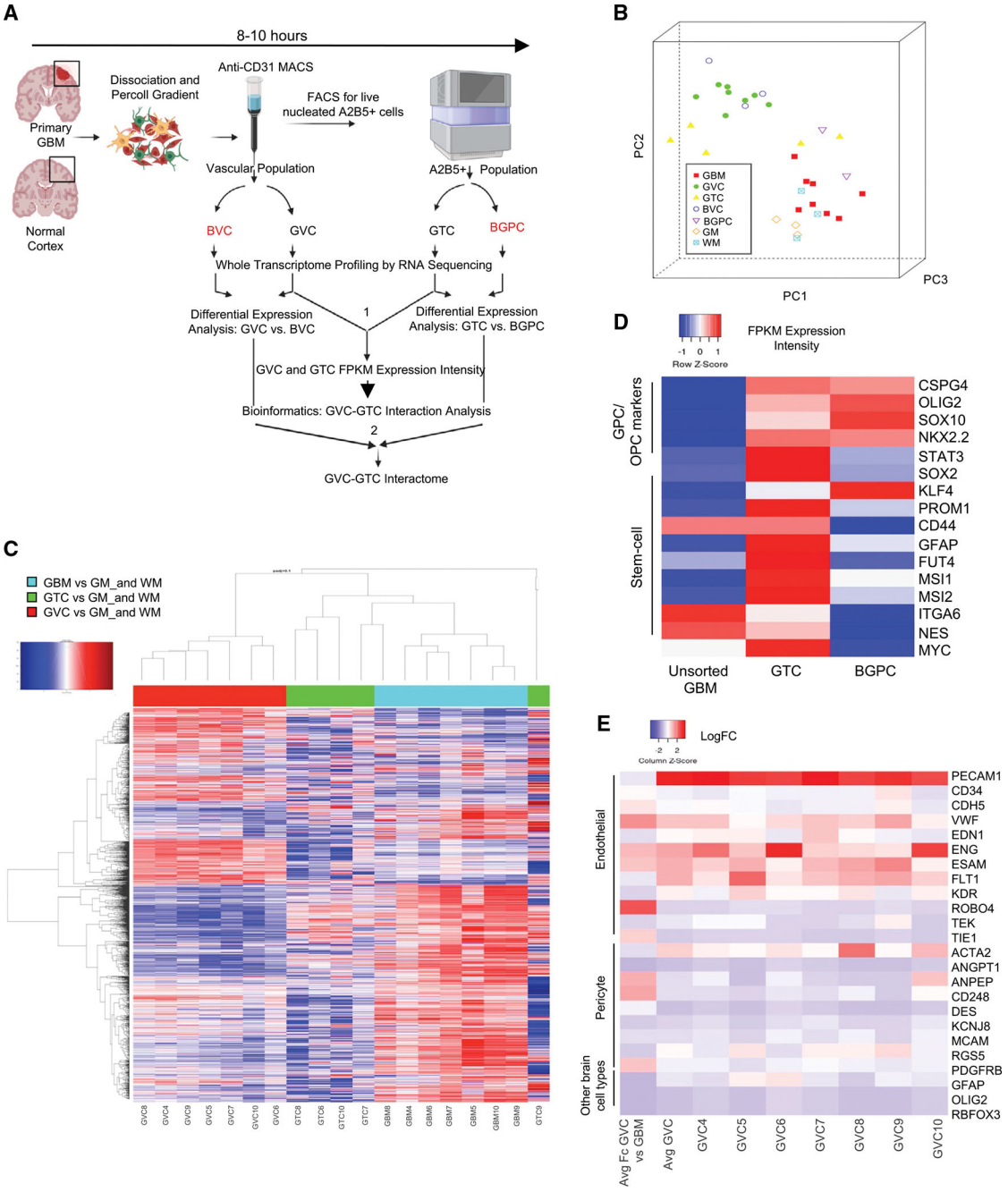

Figure 1. Transcriptomic characterization of GBM tumor and vascular cells

(A) Experimental approach for isolation and characterization of tumor and non-neoplastic cells from GBM samples and normal brain cortices.

(B) Principal-component analysis of all samples.

(C) Gene expression profile and clustering of GTC (n = 5), GVC (n = 7), and GBM (n = 7) samples.

(D) FPKM expression (FDR < 0.05) of GPC, OPC, and stem cell markers in GTCs, GBM, and BGPC samples.

(E) LogFc expression of vascular markers in GVC compared with unsorted GBM parent samples obtained through paired differential expression analysis ($p < 0.005$). See also Figure S1.

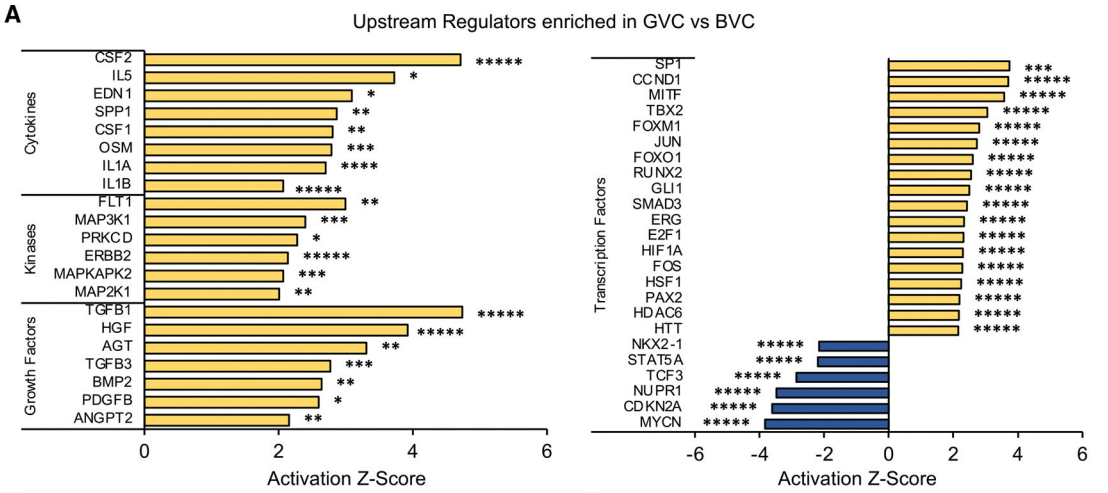

B

Diseases or Functions Annotation	Activation z-score	p-value
invasion of cells	3.27	2.8E-05
proteolysis of Gelatin	2.77	1.2E-06
mitosis	2.50	1.9E-04
activation of antigen presenting cells	2.47	1.6E-04
invasion of tumor cell lines	2.39	8.8E-04
interphase of tumor cell lines	2.39	1.7E-03
proliferation of tumor cell lines	2.26	2.2E-05
invasion of tumor	2.20	4.0E-05
mitosis of tumor cell lines	2.20	1.2E-07
quantity of connective tissue	2.17	7.6E-06
migration of cancer cells	2.12	7.9E-06
activation of blood cells	2.10	8.7E-05
invasion of tumor cells	2.08	1.8E-04
migration of tumor cell lines	2.07	6.1E-04
proliferation of cells	2.06	1.6E-10
necrosis	-2.27	1.8E-10
survival of organism	-2.31	7.9E-07
cell death of tumor cell lines	-2.54	1.6E-06

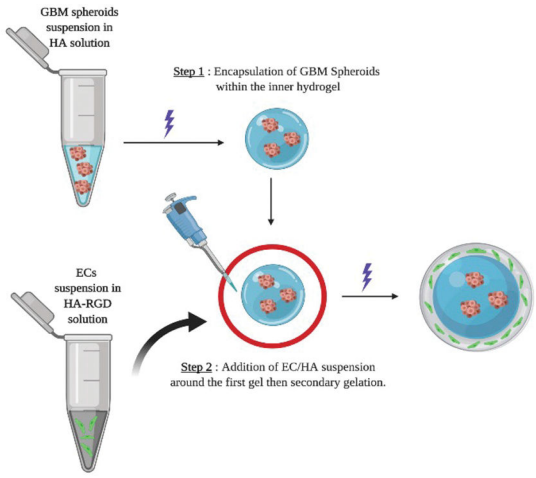

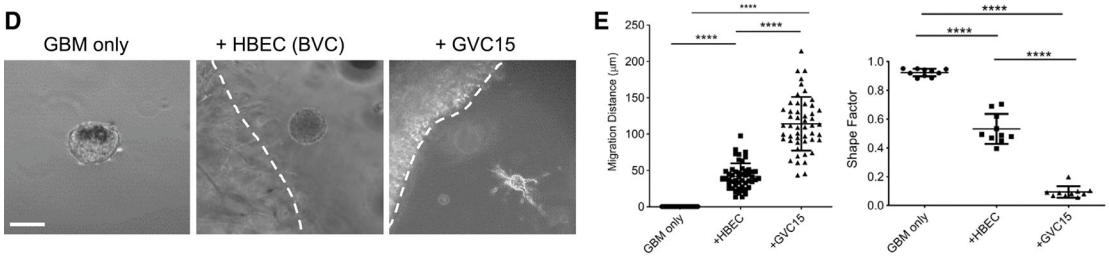

Figure 2. Enrichment of migration-related function and pathways in GVC transcriptome

(A and B) IPA analysis of upstream regulators and disease or function annotation in GVCs versus BVCs. Data are depicted as Z scores, *p < 0.05, **p < 0.005, ***p < 0.0005, ****p < 0.00005.

(C) Schematic of strategy for assessing migration in hyaluronic acid (HA)-hydrogels encapsulated with GBM and GVCs.

(D and E) Migration of GBM spheroids alone or with human brain vascular endothelial cells (HBECs) (BVCs) or GVCs encapsulated in hydrogels. The dotted line represents the boundary between the two gels. Quantitation of migration distance and shape factor. n =

10 GBM spheroids, Mann-Whitney test, **$p < 0.0001$. Horizontal bars in E represent the means, error bars represent the standard deviation. Scale bar, 100 μm. See also Figure S2.

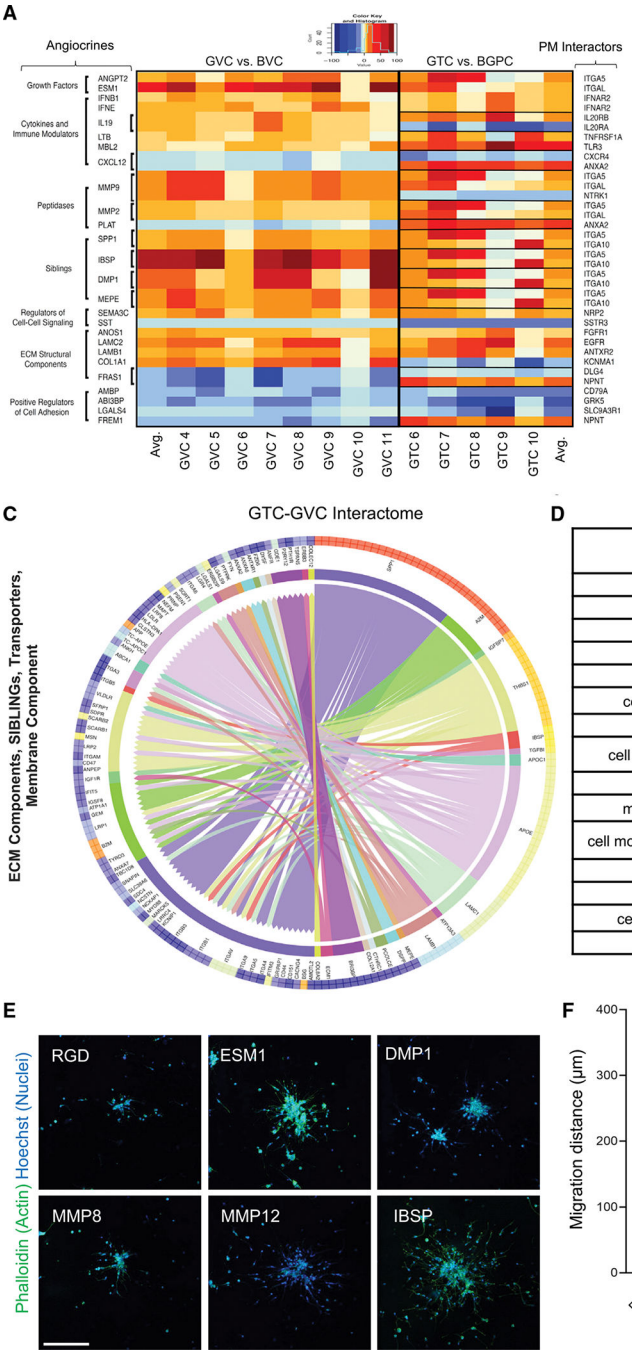

B

Diseases or Functions Annotation	p-Value
cell movement	**3.13E-21**
migration of cells	**4.38E-21**
angiogenesis	5.2E-20
vasculogenesis	3.25E-19
leukocyte migration	6.72E-19
generation of cells	3.24E-18
migration of tumor cell lines	6.68E-18
cellular homeostasis	1.19E-17
activation of cells	2.8E-17
cell movement of leukocytes	6.04E-17
cell movement of tumor cell lines	2.11E-16
proliferation of cells	2.68E-16
quantity of cells	4.24E-16
development of epithelial tissue	5.51E-16
homing of cells	6.73E-16

D

Diseases or Functions Annotation	p-value
migration of cells	**3.7E-116**
cell movement	**1.1E-109**
binding of cells	1.15E-89
angiogenesis	4.06E-88
vasculogenesis	1.02E-87
cell movement of leukocytes	3.23E-85
leukocyte migration	3.7E-83
cell movement of myeloid cells	8.91E-79
activation of cells	2.19E-78
migration of endothelial cells	1.03E-76
cell movement of endothelial cells	2.07E-75
growth of epithelial tissue	6.89E-75
proliferation of cells	6.99E-75
cell movement of phagocytes	2.07E-74
differentiation of cells	3.52E-74

Figure 3. Generation of a perivascular niche-tumor interactome

(A) Differentially regulated genes associated with GVC angiocrine-GTC plasma membrane compared with non-transformed BVCs and BGPCs.

(B) IPA diseases and functions significantly associated with the genes in the interactome.

(C) Representative circos plot of the interactome comprising ECM components, SIBLINGs, transporters, and membrane components.

(D) IPA diseases or functions significantly associated with all angiocrines and their putative GTC-PM interaction partners.

(E) Phalloidin staining of GBM spheroids encapsulated in hydrogels treated with the indicated factors. Scale bar, 100 μm.

(F) Quantitation of migration distance. n = 10 GBM spheroids, one-way ANOVA, * is pairwise comparison with RGD condition, # is pairwise comparison with rhIBSP condition. **p < 0.01, ****p < 0.0001, #p < 0.05, ####p < 0.0001. Violin plots show the median by the dashed line and the first and third quartiles by the dotted lines. The width indicates frequency distribution. See also Figure S3.

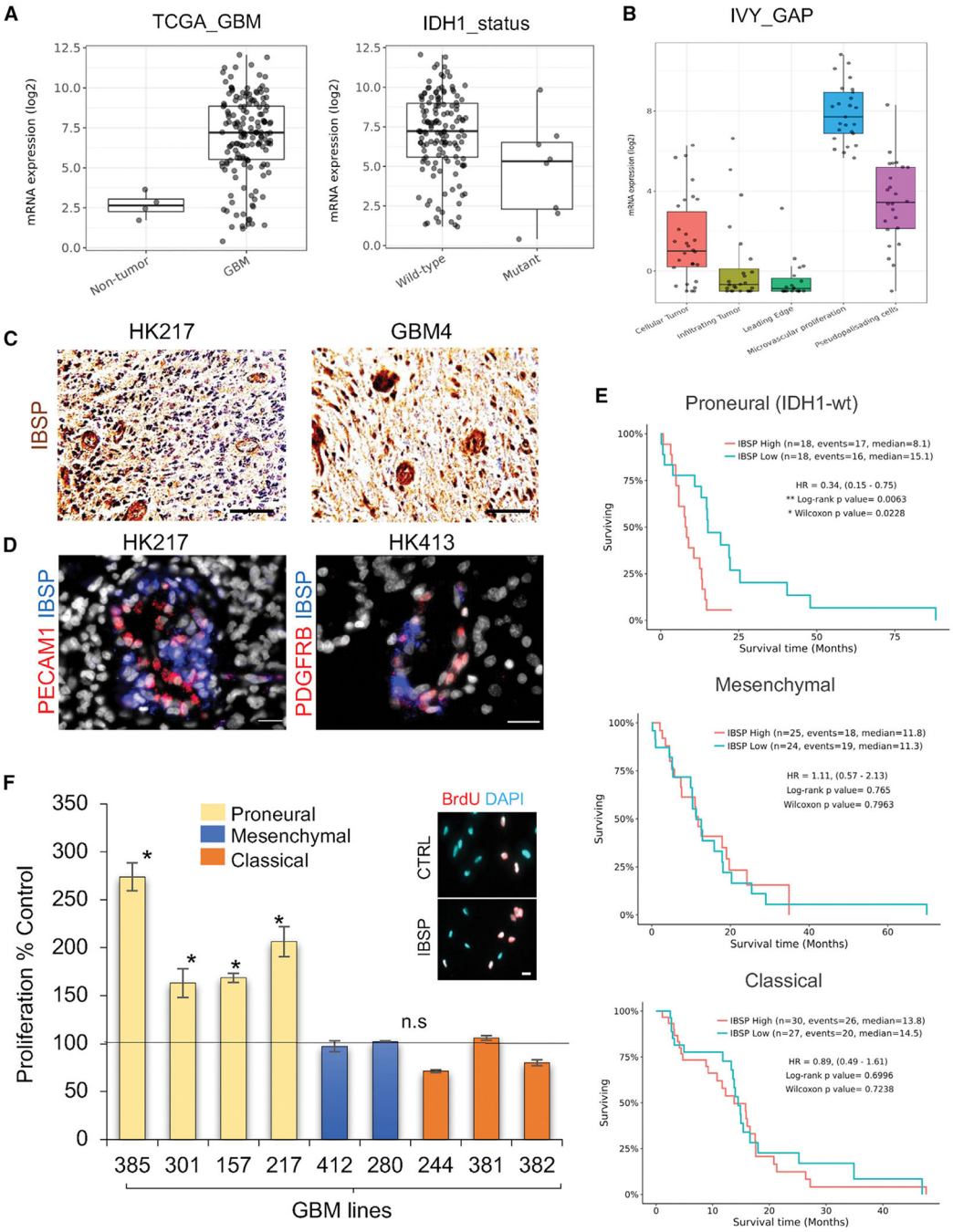

Figure 4. IBSP expression correlates with poor survival in proneural GBM

(A and B) mRNA expression of IBSP in non-tumor and tumor tissue from TCGA_GBM samples, and IDH-wild-type and mutant tumors, and in different tumor regions from the IVY_GAP database. The boxes show the lower and upper quartiles and the whiskers show the minima and maxima excluding outliers. The bar is the median value.

(C) IBSP (brown) staining in GBM patient tumors. Nuclei counterstained with hematoxylin (blue). Scale bars, 100 μm.

(D) *In situ* hybridization of IBSP (blue) with PECAM1 (endothelial, red) and PDGFRB (pericyte, red) markers in GBM tissue. Scale bars, 20 μm.
(E) Kaplan-Meier plots of patient survival correlation with IBSP gene expression in TCGA samples from each molecular subtype.
(F) Proliferation of GBM cells from the three TCGA molecular subtypes treated with IBSP shown as the mean percent control cultures plus or minus S.E.M., n = 6 independent wells. *$p < 0.05$ one-tailed paired t test. Representative BrdU (red) and DAPI (blue) staining in CTRL and IBSP-treated GBM cells. Scale bars, 20 μm. See also Figure S4.

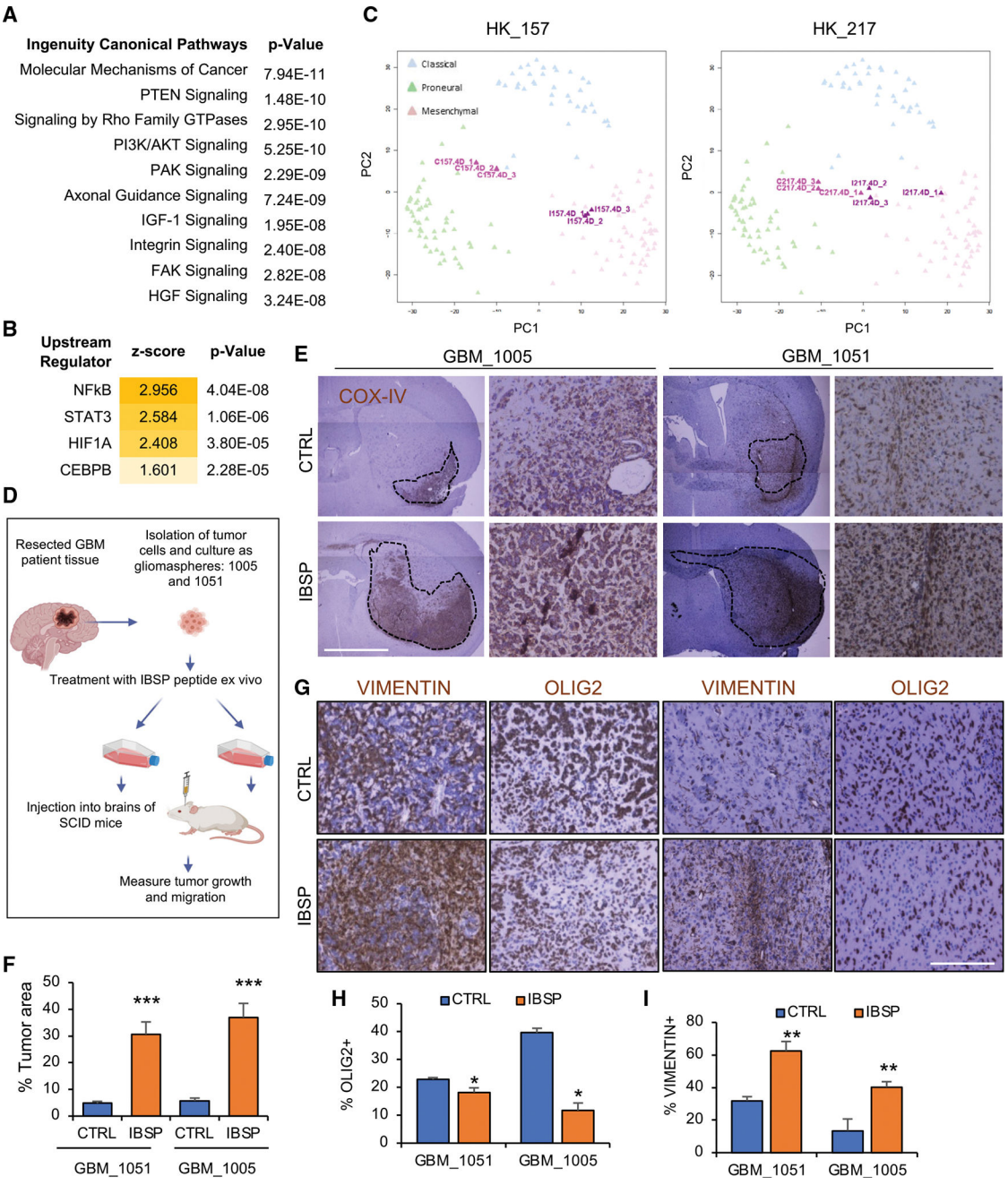

Figure 5. IBSP promotes a mesenchymal gene signature in proneural gliomaspheres

(A) Canonical pathways significantly enriched by IBSP treatment as predicted by IPA.

(B) Mesenchymal pathway regulators significantly activated in IBSP treatment (FDR < 0.001).

(C) PCA of GBM samples in the TCGA database (in background) and HK157 (left panel) and HK217 (right panel) gliomaspheres (CTRL in pink, IBSP in purple) distributed according to gene signatures used in TCGA classifications.

(D) Schematic of strategy for *ex vivo* treatment of tumor cells with IBSP in orthotopic xenografts.

(E and F) Anti-COX IV (human mitochondrial marker, brown) staining in control and IBSP-treated tumors. Scale bars, 200 μm. Quantitation of average DAB-positive tumor area per group displayed as the mean with error bars depicting standard deviation. n = 3 mice per group, **p < 0.001 and ***p < 0.0001, unpaired two tailed t test.
(G–I) Anti-VIMENTIN (mesenchymal) and anti-OLIG2 (proneural, brown) marker staining in control and IBSP-treated tumors. Nuclei counterstained with hematoxylin. Scale bars, 200 μmm. Quantitation of average DAB-positive tumor area for each marker per group. n = 3 mice, **p < 0.001 and ***p < 0.0001, unpaired two-tailed t test. See also Figure S5.

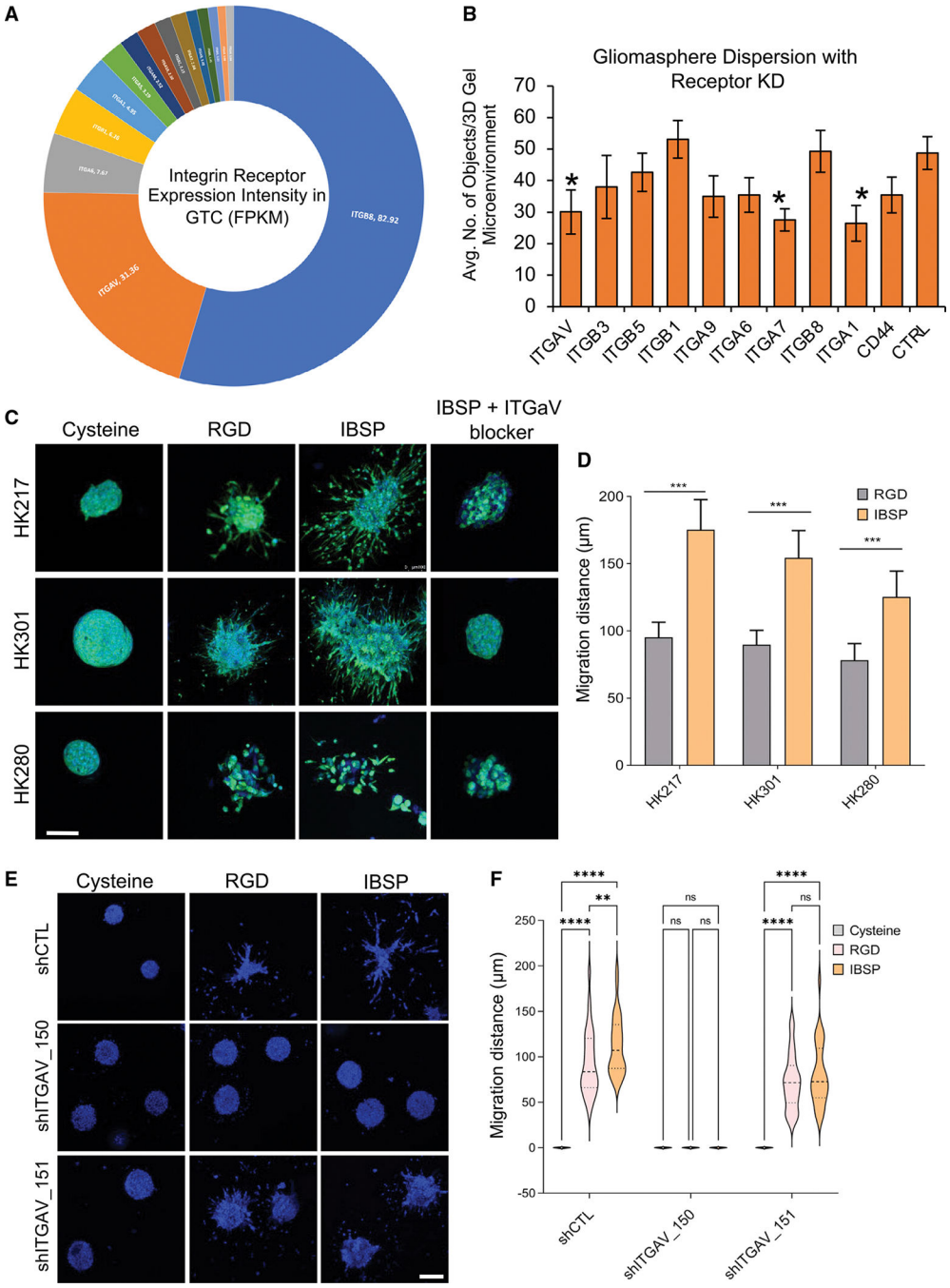

Figure 6. IBSP mediates its pro-migratory effects on GTC via ITGαV

(A) Pie chart of the FPKM expression intensity of integrin receptors enriched in GTC.

(B) Quantitation of gliomasphere dispersion in HA-hydrogels post knockdown of integrin receptors. One-way ANOVA and Tukey post-hoc test, *$p < 0.05$.

(C and D) Migration of GFP-labeled gliomaspheres from proneural GBM (HK217, HK301) and mesenchymal GBM (HK280) encapsulated in HA-hydrogels and treated with RGD (positive control) or IBSP peptides and IBSP + ITGAV-neutralizing antibody. Cysteine hydrogels were used as negative control. Scale bar, 100 µm. Quantitation of migration

distance in RGD versus IBSP treatment. n = 10 GBM spheroids, Mann-Whitney test, ***p < 0.0001. Plots in (D) are the mean plus the standard deviation.

(E and F) Migration of shITGAV-infected gliomaspheres treated with RGD (positive control) or IBSP. Quantitation of migration distance in RGD versus IBSP treatment. n = 6 GBM spheroids per group, two-way ANOVA, Tukey post-hoc test, **p < 0.01, ****p < 0.0001. Violin plot shows the frequency distribution with the median indicated by the dashed line and the first and third quartiles indicated by the dotted line. See also Figure S6.

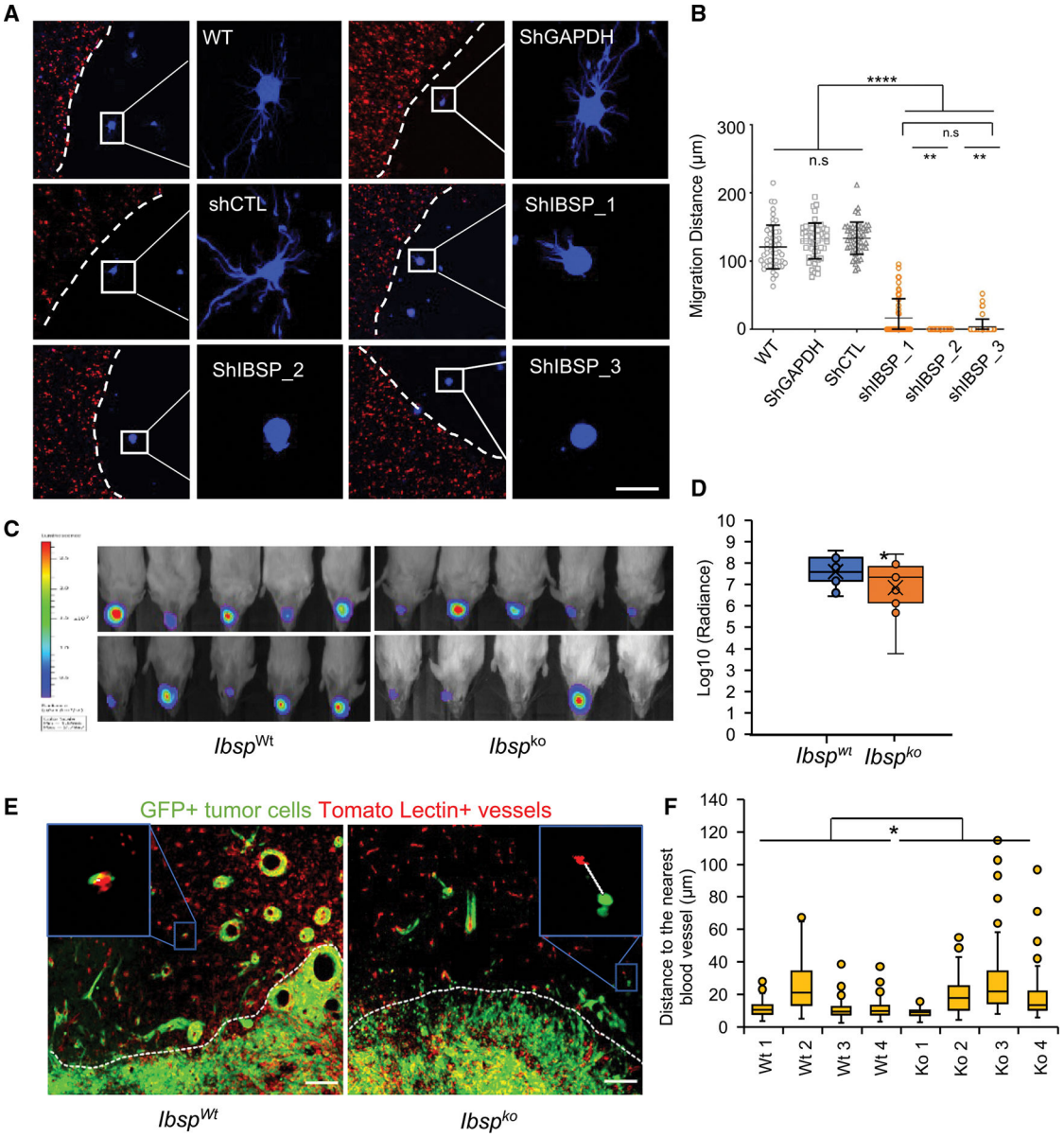

Figure 7. Endogenous vascular cell-derived IBSP promotes GBM growth and migration

(A and B) Migration of GBM spheroids (BFP, blue) with IBSP-deficient GVC (shIBSP) or control (shGAPDH, and shScrambledCTL) GVC (mCherry, red). White dashed lines demarcate the two hydrogels. Boxes show higher magnification images of the GBM spheroids. Scale bars, 250 µm. Quantitation of migration distance. n = 10, one-way ANOVA and unpaired t test, **p < 0.0001.

(C and D) Images show luciferase signal from murine GBM tumor cells implanted into *Ibsp* knockout ($Ibsp^{ko}$) and wild-type ($Ibsp^{wt}$) mice. Quantitation of tumor growth measured by luminescence. n = 10 mice per group and *p < 0.05, unpaired two-tailed t test.

(E) Anti-GFP (tumor cells, green) and anti-Tomato lectin (blood vessels, red) staining in *Ibsp* knockout and WT mice. White dashed lines show the tumor edge. Boxed inlets show association of GFP + tumor cell with lectin + blood vessel. Scale bars, 100 µm. Edges of

the box represent 25th and 75th percentiles, the middle line represents the mean, and the x represents the median value. Whiskers represent 95% confidence intervals.
(F) Quantitation of log normalized distance of tumor cells from blood vessels in each group using a linear mixed effects model. Knockout (KO) mice have higher mean distance compared with WT mice (log normalized average of 0.71, SE = 0.31, p = 0.02). Edges of the box represent 25th and 75th percentiles and the middle line represents the median value. Whiskers represent 95% confidence intervals. Dots represent data points that exceed 1.5 times the inner quartile range. See also Figure S7.

KEY RESOURCES TABLE

REAGENT or RESOURCE	SOURCE	IDENTIFIER
Antibodies		
Mouse monoclonal anti- CD31, JC70A, human	Agilent DAKO	Cat#: M082329-2; RRID:AB_211471
Anti-human CD31 antibody, REA730	Miltenyi Biotec	Cat#: 130-110-670; RRID:AB_2657283
Rabbit polyclonal anti-GFP	Novus Biologicals	Cat#: NB600-308; RRID:AB_341929
Mouse monoclonal anti-mCherry	Novus Biologicals	Cat#: NBP1-96752; RRID:AB_11034849
Chicken polyclonal anti-GFP	Novus Biologicals	Cat#: NB100-1614; RRID:AB_10001164
Chicken polyclonal anti-mCherry	Millipore Sigma	Cat#: AB356481; RRID:AB_2861426
Tomato Lectin-DyLight 649	Vector Laboratories	Cat#: DL-1178-1
Anti-A2B5 antibody, clone 105	ATCC	Cat#: CRL-1520; RRID:CVCL_7946
Anti-IBSP antibody, LFMB-25	Santa Cruz Biotechnology	Cat#: Sc-73634; RRID:AB_2121524
Anti-ITGαV antibody	Abcam	Cat#: Ab16821: RRID: AB_443484
Anti-COXIV antibody	Cell Signaling	Cat#: 4850; RRID:AB_2085424
Anti-VIMENTIN antibody	Cell Signaling	Cat#: 5741; RRID:AB_10695459
Anti-OLIG2 antibody	Abcam	Cat#: Ab109186; RRID:AB_10861310
Anti-CD44 antibody	Cell Signaling	Cat#: 3570; RRID:AB_2076465
Anti-YKL40/CHI3L1 antibody	Abcam	Cat#: Ab77528; RRID:AB_2040911
Bacterial and virus strains		
pLV-FireflyLuc-GFP	UCLA Vector Core	N/A
pLV(EXP)-puro-EF1A-mCherry	Vector Builder	N/A
pGIPZ_puro_shRNA_IBSP	Horizon Discovery	VHG5518, clones V2LHS_61769, V3LHS_334208, V3LHS_334212
pGIPZ_puro_shRNA_ITGaV	Horizon Discovery	VHG5518, clones V2LHS_133468, V3LHS_365150, V3HLS_365151
Biological samples		
Human Primary GBM patient tumors	This paper	N/A
Pediatric human brain cortex samples	This paper	N/A
Chemicals, peptides, and recombinant proteins		
Percoll	Sigma-Aldrich	Cat#: E0414
Collagenase II and IV	Worthington Biochemical	Cat#: LS004174, LS004186
Hibernate A minus Ca, Mg	BrainBits LLC	Cat#: HACAMG500
Endothelial cell media	Sciencell	Cat#: 1001
Endothelial cell media (EGM-2)	R&D systems	Cat#: CCM207
Anti-human CD31 Dynabeads	Thermofisher Scientific	Cat#: 11155D
RGD peptide	Genscript	Cat#: RP20297
Recombinant Bone Sialoprotein (IBSP)	Abcam	Cat#: ab219248
Recombinant Lumican	Abcam	Cat#: ab114635
Recombinant InhibinB-A	Abcam	Cat#: ab53506

REAGENT or RESOURCE	SOURCE	IDENTIFIER
Recombinant WNT5A	Abcam	Cat#: ab204627
Recombinant IBSP	R&D systems	Cat#: 4014-SP-050
Recombinant Endocan	R&D systems	Cat#: 1810-EC-050/CF
Recombinant DMP1	R&D systems	Cat#: 4129-DM-050
Recombinant MMP8	R&D systems	Cat#: 908-MP-010
Recombinant MMP12	R&D systems	Cat#: 917-MPB-020
Critical commercial assays		
Vectastain Elite ABC-HRP, DAB Kit	Vector Laboratories	Cat#: PK6100, and SK4100
TSA Plus Cyanine 3 System	Perkin Elmer	Cat#: NEL744001KT
TSA Plus Cyanine 5 Evaluation Kit	Perkin Elmer	Cat#: NEL745E001KT
Dil-Ac-LDL assay	Cell applications	Cat#: 022k
CCK8 assay	Dojindo Molecular Technologies	Cat3: CK04
CellTiter-Glo Luminescent viability assay	Promega	Cat#: G7570
Deposited data		
RNA-sequencing data (raw and analyzed)	This paper	GEO Accession number: GSE186932
Microarray data (raw and analyzed)	This paper	GEO Accession number: GSE186932
Experimental models: Cell lines		
Patient-derived gliomasphere lines	This lab	N/A
Human Brain microvascular endothelial cells (HBEC/BVC)	Sciencell	Cat#: 1000
293T packaging cells	ATCC	Cat#: CRL-11268
Murine GBM line	Dr. Maria Castro	Nunez et al., 2019
Experimental models: Organisms/strains		
NOD.Cg-*Prkdc*^{scid} *Il2rg*^{tm1Wjl}/SzJ (NSG)	Jackson Laboratory	Cat#: 00557
IBSP knockout mice (Ibsp^{tm1Jeau}/Ibsp^{tm1Jeau}), 129/SvJ-CD1 background	Martha Sommerman and Harvey Goldberg labs	Malaval et al., 2008
Oligonucleotides		
Human primers listed in Table S6	This paper	Integrated DNA Technologies
Recombinant DNA		
N/A	N/A	N/A
Software and algorithms		
Ingenuity Pathway Analysis (IPA)	Qiagen	www.ingenuity.com
STRING: functional protein association networks	STRING	http://string-db.org
R-bioconductor-package	The R project for Statistical computing	http://www.bioconductor.org

REAGENT or RESOURCE	SOURCE	IDENTIFIER
R-combat package	The R project for Statistical computing	http://statistics.byu.edu/johnson/ComBat; 16632515)
Database for Annotation, Visualization and Integrated Discovery	DAVID	https://david.ncifcrf.gov
GSEA	Broad Institute	href="http://software.broadinstitute.org/gsea/index.jsp
Image J	National Institute of Health	https://imagej.nih.gov/ij/
GraphPad Prism 9	Graphpad	https://www.graphpad.com/scientific-software/prism/
Biorender	Biorender	https://biorender.com/